Integrated M.Sc. Thesis

Submitted to

UM–DAE

Centre for Excellence in Basic Sciences

Study of Resonances in ^{12}C

Sanchit Sablok

Thesis Guide:

Dr. Hans O. U. Fynbo

Aarhus University, Denmark

External Examiner's Signature: _____

Thesis Guide's Signature: _____

Abstract

The primary objective in this project is to complete a scan of the states in ^{12}C in the energy range 16.4 MeV to 19.5 MeV by using protons with energies in the range 500 keV to 3500 keV with variable step size of incident proton energy. While previous studies have been carried out to look at the above states, the current study is the first of its kind to look at the states with the commissioned detection setup. The experiment is the first step towards looking for new gamma decays in the ^{12}C nucleus in the above energy range. Once the resonances are established, longer runs can be taken at an individual resonance to look for evidence of previously unseen gamma transitions.

The 5 MeV Van de Graaff accelerator at Aarhus University was used to produce proton beams for the experiment. The target was ^{11}B on a carbon backing. The detection setup comprised of 2 square and 2 annular ring Double Sided Silicon Detectors surrounding the target. Contrary to previous experiments where the resonances were detected using gamma rays, the setup used in this experiment looks for charged particles. As such, it can detect triple alpha coincidences which are seen in this reaction. The coincidences are verified to originate from a single decay event by calculating the total energy & momentum of the coincident alphas. These are then constrained to conserve energy and momentum. To get the cross section, the ratio of alphas obtained is compared with an output simulated using Monte-Carlo techniques with known number of decays.

The differential cross sections have been computed for the above reaction for various energies. Selected results are shown at the end of the report.

Preface

This project report has been compiled based on the work I have done at Aarhus University in the period of July – November, 2016 with the Nuclear Physics group under the supervision of Dr. Hans Fynbo.

Indebted to CBS for having engrained the culture of writing lab reports every semester, I have found this task far less daunting than certain peers in my position would envisage. In addition, the added experience of having written two project reports in the previous two semesters has provided an added depth to my own style of writing. I have tried my best to incorporate the advice of all my mentors along the way, while trying to maintain my own distinct style of writing.

Unlike my previous attempts, this is not a dry description of facts and results. Instead, in this endeavour, I have strived to narrate the journey I undertook. Five months is not a long time in the realm of scientific effort and I have tried to learn and do as much as I could, given the constraints imposed by time and the attention demanded by other practical matters.

The project had queer beginnings as the month of July is apparently when most of Denmark goes on vacations. Left alone in the lab with Jacobus (Cobus) Swartz, I had been instructed to complete a scan of the $^{11}B(p,\alpha)2\alpha$ reaction. All the details pertaining to running the 5 MeV accelerator at the laboratory had been provided in the first week of my stay. At the time, the task felt daunting, more so due to the lack of anyone else for support than the task of taking the measurements. I soon discovered that I was never really alone. Oliver, Michael and Hans were all an email away and made my task all the more easy.

I was soon to realise that the hard part was yet to come. This began when I first encountered the analysis framework AUSAlib, the library developed by the group to handle their analysis. Being inept at C++ and ROOT at the beginning, I struggled to distinguish if a piece of code was C++, AUSAlib or ROOT based (even though ROOT and AUSAlib are both essentially C++). After a lot of reading, sample coding and a giant helping hand in the form of Oliver's own code I could play around with, I could finally start analysing my data. However, new issues in the form of calibration and shifting objectives kept coming up. Every minor digression turned out to be longer than imagined and come September, I had used up a lot of time with little progress to show for it. At the same time, AUSAlib was undergoing a major upgrade, with the analysis being split into two individual components, the Identifier and Event Builder.

Having completed the calibrations (to the best of my ability), October arrived with the promise of cold and work. Balancing studies for GRE, surfing for PhD applications and working in the laboratory was hard enough already, but now I had warmed up to my new friends and Denmark and my social life was taking a turn for the better! All of this added up to a rather hectic dash to the finish line towards the end as I had to eventually use SimX, the simulations program developed at Aarhus to finalise my results.

The objectives we set out to accomplish have not been fully realised and ideally I would like to continue to work on them. However, that is a topic to discuss for another day. I hope you find this report not only instructive and succinct but also fluent and easy to understand.

Acknowledgements

At the outset, I would like to thank the never ending support of my parents, who made it possible to be able to apply for this project in the first place and then helped me over the line with their love and encouragement.

I owe a massive debt of gratitude to Hans, for having picked me out of the haystack of applicants to work with the group. From teaching me how to run the accelerator, to showing me how to run a 5 km race, I have had a learning experience and made some memories to last for a lifetime, all thanks to him.

To all the members at the nuclear physics group at Aarhus – Oliver, Michael, Cobus, Jonas, Jesper and Karsten – I am truly indebted for having welcomed me like one of their own and provided invaluable support and guidance at all times. A special tip of the hat to Oliver and Michael, who I tried my best to annoy with countless mails filled with questions, but seemingly, never could.

To my housemates in Aarhus – Christian, Andreas, Pernille and Camilla, who will probably never read this – thank you for introducing me to the Danish culture and having borne with my childish tantrums for months. Aarhus would have been much colder without you guys!

Lastly, this report would not be possible without some important contributions by Abhinav, whose invaluable help when needed the post, was much appreciated.

The project was partially funded by the Innovation in Science Pursuit for Inspired Research (INSPIRE) fellowship.

Table of Contents

Introduction

"A journey of a thousand miles starts beneath one's feet..."
- Laozi

It all started with Ernest Rutherford's discovery of the nucleus way back in 1911. It has been more than a century and nuclear physics has come a long way since. Like many other fields in science, nuclear physics has benefited from the tremendous growth in technology over the last few decades. The story of this project is one such narrative where the advances in technology have spurred new experiments and resulted in new insights into the nuclear structure. The experiment itself is quite simple and old in its conceptualisation. However, what is modern is the execution.

Motivation

The reaction $^{11}B(p,\alpha)2\alpha$ is important from several distinct point of views. It results in formation of the unstable $^{12}C^*$ nucleus which decays into 3 alpha particles. This process occurs in two steps, the first being the emission of 1 alpha particle which leaves behind ^{8}Be. This nucleus can then decay further emitting two more alpha particles. The details of mechanism of this reaction have implications ranging from astrophysics to material science.
Fred Hoyle predicted the now famous Hoyle State (1) in ^{12}C which is important to understand Helium burning process inside stars. Since it is difficult to study the process of triple alpha fusion in the laboratory, we study the inverse process, which is the decay of ^{12}C into three alpha particles using the $^{11}B(p,\alpha)2\alpha$ reaction. Such studies have been previously carried out by Segel, et al. (2), Davidson, et al. (3) and Becker et al. (4). Note that while this project is a study of this process, the exact state through which ^{12}C is decaying is not the Hoyle state. The study of this process is also important to calculate the reaction rates in stars, which can tell us more about their life cycles (5).
A second motivation to study this reaction is due to its potential to be used in a nuclear fusion reactor. The reaction is favoured since it releases its energy in the form of energetic alpha particles. No neutrons or gamma radiation is emitted in this reaction. Such "aneutronic" fusion reactors (6) (7) (8) are advantageous over their counterparts due to the fact that excess neutron radiation can cause damages due to neutron activation. Thus, they require better shielding and safety protocols than when dealing with charged ions.
Lastly, detailed knowledge of the cross section of this reaction can help to identify traces of ^{11}B in a material (9). Even though such identification hinges on assumptions of homogeneous distribution in the material, they are nevertheless an advantage over other methods.
This study is based on my work and understanding of the above reaction as well as the detection setup and data analysis framework that was used to analyse the data.

Experiment

The 5 MeV Van de Graaff accelerator at Aarhus University was used to produce proton beams of a given energy. This beam was used to bombard the ^{11}B target in a vacuum chamber. The target was surrounded by two annular ring Double Sided Silicon Strip Detectors (DSSSDs) and two square DSSSDs. Each detector has a large solid angle coverage (of the order of ~ 10%). So the detection setup as a whole covered a large solid angle. Since the detectors are all detecting alpha particles, they have a very high efficiency. The unique nature of the detection setup however, comes from the fact that the data acquisition and analysis system can detect all three alpha particles from the $^{11}B(p,\alpha)2\alpha$ reaction. Thus, any ambiguity in the number of decay events in the target is removed as was the case in previous investigations by Davidson, et al. and <Cite the other paper>.
The experimental data analysed in this report consists of a total of 35 runs, which were of approximately 1 hour duration each over the course of 3 weeks in July. Each run is characterised by the incident proton energy. The objective was to study the reaction rate and differential cross section as a function of incident proton energy. Since several resonances were already known in this

energy range, the incident energy of protons was varied keeping in mind the width and positions of known resonances.

Data analysis is carried out using the AUSAlib analysis framework which is abbreviated for Aarhus University Subatomic Library. AUSAlib is a library designed primarily by Michael Munch, Oliver Kirsebom and Jesper Halkjær. The methods in AUSAlib are designed on the ROOT framework or in C++ 11. AUSAlib was used to develop a standard procedure for analysing data keeping ease of work and utility in mind. These are described in detail in the chapter on Data Analysis.

Experiment

Setup

The 5 MeV Van de Graaff accelerator at Aarhus University was used to produce the proton beam required for the experiment. While the accelerator can in theory produce a beam up to 5 MeV in energy, in practice it was not used above 3.5 MeV to avoid electrical breakdown.

A Van de Graaff accelerator uses a moving belt to accumulate charge on to a metal globe. This accumulation of charge produces an electric field which can be used to accelerate particles. However, since there is a very high electric field associated with this kind of acceleration, this cannot be done in open air. Hence, the accelerator is kept inside a sealed chamber which is flooded with SF_6 gas. SF_6 has a breakdown voltage 3 times higher than air. So, it can sustain fields of up to ~ 9 MV in theory. In practice, there have been known breakdowns with this particular accelerator at voltages of ~ 4 MeV or above. So, caution was advised and the advice was heeded.

The detailed electronics of the internal workings of the accelerator were not the subject of this study and hence are not discussed in great detail. Having obtained the beam, it is focussed onto the target with the help of deflector plates and slits. Caution has to be exercised in focussing of the beam since too much beam current could cause the target to break. As a precaution, the beam is obtained and focussed onto a collimator which has a diameter of 2 mm. The beam current is measured with the help of a Faraday Cup placed 70 cm downstream, which is connected to a beam digitiser. This beam current can be monitored through while focussing the beam. Typically beam currents of the order of a few hundred pAmps were used.

The target comprises of a thin film of ^{11}B deposited on a carbon backing. The thickness of the target was determined to be 12.6 +- 1.2 µg/cm^2. The target is deposited on a carbon foil of thickness ~ 4 µg/cm^2. The target thickness was determined by bombarding the target with a Helium beam at 0° and then at 180°. This run was then analysed to find the backscattered elastic peak off carbon. The shift in energy corresponds to twice the energy loss in the target foil. This energy loss is then used to find the target thickness using the following expression –

$$d = \frac{E_0 - E_{180}}{k(\theta)^2\, S(E_{beam}) + \dfrac{S(k(\theta)^2[E_{beam} - S(E_{beam})d])}{\cos\theta}}$$

Equation 1

Where, d is the thickness of the foil,

k(θ) is kinematic factor

S is the stopping power and

θ is the scattering angle relative to normal direction of the foil.

In the calculation done for this particular experiment, the stopping power due to initial energy loss was neglected (effectively setting d = 0 on the RHS) thus the expression did not have to be solved iteratively. A deposit of some sorts was seen on the target at the end of the experiment. There was some evidence that this could be carbon built up from the reaction but this was not confirmed. However, it was made sure that this build up will not have a considerable effect on the analysis.

Figure 1 – Picture of the Target Ladder. The target used is the one on extreme right, which is a natural ^{11}B target deposited on a foil with Carbon backing.

The target is placed on the target ladder, as seen in Figure 1, which can be raised and lowered in height by a discrete amount. A maximum of 5 targets can be placed on the ladder. This allows us to change targets without venting and evacuating the chamber again, saving valuable time. The target ladder is shown in the picture. The ^{11}B target was loaded as the lowermost target which enhanced data quality since there was no shadowing of the beam from the ladder as is the case for the 4 target positions above. This picture was taken after the experiment. The small black spot is where the beam was concentrated throughout the reaction and has led to build up of ^{12}C presumably. The beam spot thickness is approximately 2 mm to give an indication of size of the target.

The target is surrounded by the two square W1 and two annular ring S3 DSSDs. A schematic of the detector setup is shown below. This image has been generated using the 'Drawer' utility in the AUSAlib library. The utility requires the setup file to draw the detection setup. One can also adjust the camera angle at which the drawing is rendered.

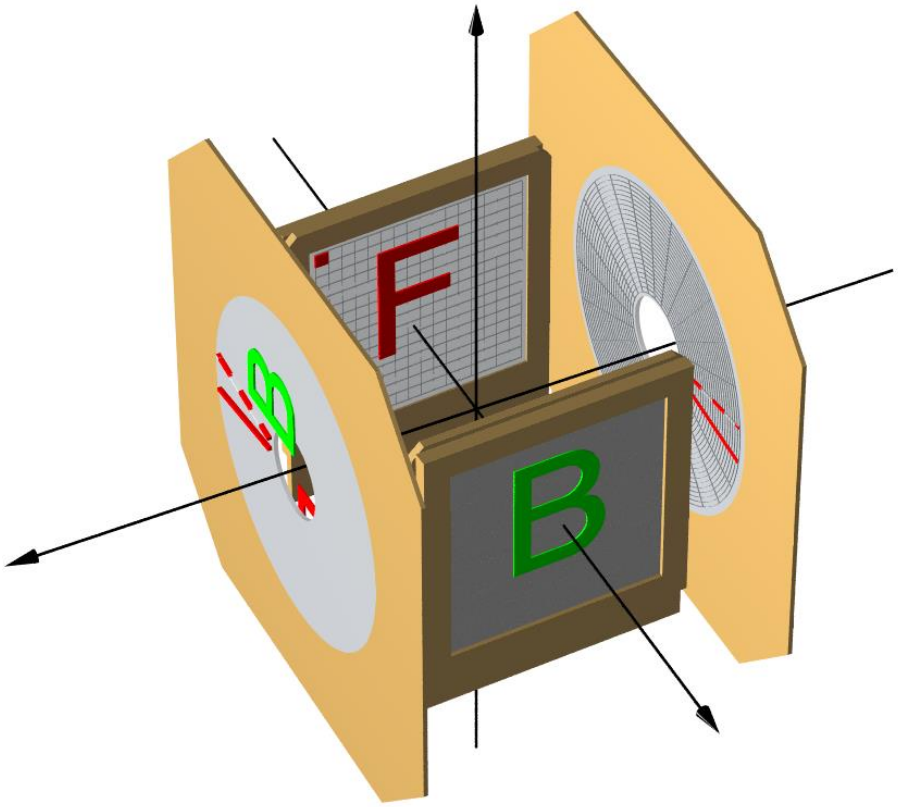

Figure 2 – Detector Placement. The beam passes through the S3 Detector.

As can be seen from the figure, the beam enters through one of the S3s and hits the target placed at the centre of the setup. The reaction products are detected using the detectors placed around the target.

The details of the two different detectors are discussed here. Consider the two figures shown below.

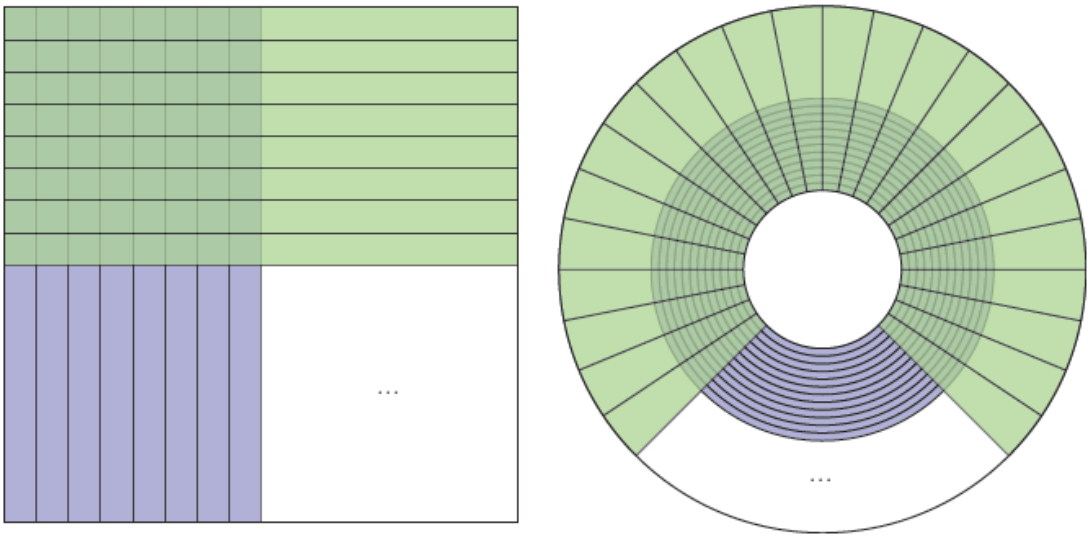

Figure 3 – (Left) Square W1 DSSD (Right) Ring S3 DSSD

Figure 3 (left) illustrates the W1 detector whereas Figure 3 (right) illustrates the S3. Both the detectors are DSSDs, or Double Sided Silicon Strip Detectors. This implies that charge collection is done using strips on both sides of the detector. So, the front strips on both detectors are orthogonal to the back strips. Moreover, the front and back strips have opposite polarities so that if one collects electrons, the other collects holes. The W1 detector measures 5 cm × 5 cm and has 16×16 strips. These are labelled front (F) and back (B) strips for the purpose of analysis. Each individual strip has a thickness of 3 mm and an inter-strip width of 0.1 mm. The S3 detector on the other hand has an inner diameter of 22 mm and an outer diameter of 70 mm. The strips on the S3 are labelled as rings (R) and spokes (S). The S3 has 24 rings and 32 spokes.

Data Acquisition

The Data acquisition is briefly described in this section. However for the purpose of this report, I will not be going into the details of the mechanism.

Consider a single charged particle which deposits energy in the detector. This energy is deposited in the form of multiple electron-hole pairs created in the silicon detector. The energy required to create one electron hole pair in the silicon is nearly 3.62 eV (10). So, for a particle of energy of the order of MeV, approximately 10^6 e^- /hole pairs are created. These are collected and have a total charge of the order of 0.1 pC. This is an extremely small signal and can be distorted due to electronic noise. So, the first requirement is to amplify this signal very close to its origin.

The preamplifier is used for this purpose. An integrator circuit converts this charge into voltage. This gives the initial pulse whose voltage is proportional to energy of incident particle. The Mesytec MPR32/64 charge amplifier (11) was used for this experiment.

Once we have the initial signal, it goes through the amplifier. The amplifier serves a dual role. Firstly, it amplifies the signal so that the voltage of the signal is in a range where it can be passed through the digital components down the line. Secondly, the amplifier shapes the pulse, which improves the signal to noise ratio. Once amplified, a signal has a tail of 3-4 microseconds. This sets a limit on the maximum rate of which particles should be bombarding the detector. If there is more than one signal within this time frame, the signals would sum and give incorrect energy. However, this is not a very big problem in the current setup since we have segmented the detector into strips. As a result,

we don't get pileup until and unless we have two particles incident on the same front and back strips. If the two are incident on the same front strip but different back strips, the process of matching eliminates the problem. Thus, the rate during the experiment was limited to nearly 10 kHz. The amplification was done with the Mesytec MSCF-16 (12) Module.

Once amplified, a signal goes through a discriminator. The Mesytec STM16+ (13) module is used for this. This is done to filter out any signals due to noise. Two techniques are used. First is leading edge discrimination, which compares the signal to a fixed threshold and the second is constant function discrimination, which finds the maximum of the signal by finding where the slope of the signal goes to zero.

This step gives the signal which now passes through the Analog to Digital Converter to be digitised. The CAEN V785 (14) is used for this.

To do this conversion, a capacitor is charged with a constant current while input signal potential is greater than capacitor potential. The Potential on capacitor is then digitised. After this step, the capacitor needs to discharge before a new signal can be accepted, thus in this time frame, the module does not accept new events. This time is of the order of 5 to 7 μs which sets the limit of maximum acceptable event rate at about 100 kHz.

All signals are time-stamped using the CAEN V1190 (15) Time to Digital converter. This particular module uses a combination of counting clock cycles and interpolation.

Finally, we need to know the total charge deposited by the beam to calculate cross section. This is done using the CAEN V830 (16) scaler module which gives a logic true signal for every 10 pC deposited by the beam.

Analysis Framework

Once data is acquired it is stored in the RAW files which can be unpacked to a ROOT file using the ucesb tool (17). This ROOT file is the data file which is taken for analysis. Refer to the figure for schematics of the data analysis.

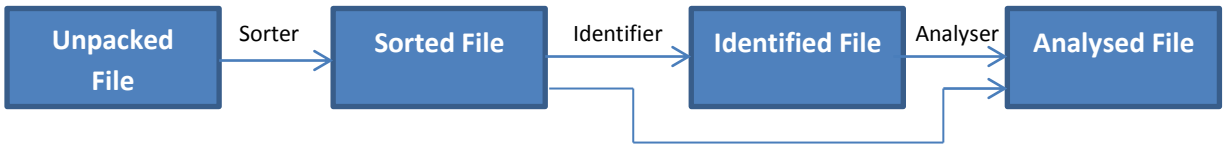

Figure 4 - Data Analysis Schematic

Sorter

Sorting is the first step of the data analysis. It does the task of calibrating and matching the unpacked data.

Calibration

The process of calibration assigns an energy value to each recorded event based on a number of inputs. These are defined previously in a set of files which are briefly described below:

a. Setup file: This is a text file which contains information about the detection setup. The information in the setup file is listed as follows:

- The geometry configuration of all the detectors in the setup. This has to be entered manually after geometry calibration.
- The types of Detectors.
- Detector Calibration files obtained from energy calibration.
- Files containing detector properties such as thickness, dead layer thickness, disabled stripes etc. It specifies the naming conventions for the sorted file.

b. Calibration files: Each detector has an associated text file with a ".cal" extension which contains the energy calibration for each strip. This is simply a text file with two columns containing slope and intercept for each individual strip (front and back) in the detector.

c. Detector files: Each detector has an associated ".json" file. This is a test file with important parameters such as dead layer thickness, disabled strip etc. for each detector. This is important for energy loss corrections in the analysis.

Matching

Requires a "matcher.json" file to function. The purpose of this step is to match front and back strip hits. The front and back strips have opposite polarity. So, one set of strips collect electrons while the other collects holes. For a single particle, there will be charge collected on one front strip and one back strip (Ignoring the case when particle hits inter-strip areas). The energy difference between the two is taken and a threshold can be set for the minimum energy difference that is acceptable for a pair. This information is provided in the "matcher.json" file.

For more than one hit, energy differences between all possible pairs are considered and the ones with minimal energy difference are accepted. This works in majority of the cases.

The case where the particle hits the inter-strip area is ignored because, as previously mentioned the surface area covered by inter-strip distance is nearly 1%. Moreover, thickness of the strip is 3 mm compared to few 10s of a µm needed for protons or alphas to deposit energy.

Identifier

This is the second stage of Analysis. The identification requires the output of the sorter (a "matched" file) as its input.

The Identifier then takes this file and gives an identified file as an output which is also ROOT file with a determined Tree Structure. The primary function of the Identifiers is the identification of the particles detected. However, this is not arbitrary. The user specifies exactly which particles are expected in the given reaction. The Identifier then considers each hit and consults a set of criteria to determine whether the given hit can possibly correspond to the list of particles specified by the user. If the criterion is met, the identifier assigns to the hit corresponding particle ID and cycles through.

Consider this example. Let a hit register on a W1 detector. After sorting, the energy & position of this hit is known. In the context of this particular experiment we are only looking for either protons or alphas. So, the identifier checks if the particle can be a proton or an alpha. This is done by considering a proton or alpha can deposit the energy in the detector, since we know the rate of energy loss for both is different. So, for a given thickness of a detector, a proton and alpha both have a maximum value of energy which can be deposited.

A second method of Identification could be a dE-E cut by placing a pad detector behind a DSSD, but this has not been implemented in this experiment since the pads were not used by this experiment.

Once the Identification is complete, the identifier enters the details of the hit along with the identity of the particle for each hit. Note that this could result in a hit being classified as both a proton and an alpha in our example. Hence, the identifier acts like a sufficient but a necessary condition for a hit to be a given particle.

The identifier is a highly useful and versatile tool. Other than particle identification, it also carries out an energy loss correction assuming the identified particle (Since particle type is needed for energy loss calculations) in the target as well as dead layers.

The advantage of using the identifier is the ease and speed of analysis. Previously, the energy loss corrections and identification were part of Analysis. However, these are time consuming steps which need not to be done only once for a given file, given all the calibration data. Separating the Identifier from the analysis saves significant amount of time in analysis. Now, small changes in analyser code, which is modified frequently, can be rapidly tested. The Analysis time has come down from approximately 4-5 minutes per run (of approximately 1 Hour) to under 30 seconds, which is a factor of 10.

Analysis

The analysis is the final stage of analysis and requires both the sorted and identified data as its input. The analyser is the part of the analysis framework which is highly specialized for a given experiment and is usually authored by a specific person in the group. I have written the code for analysis of this experiment based on valuable input from Michael Munch as well as Oliver Kirsebom.

The analysis is set-up to do the following. Since it is known that the reaction can proceed through the ground state or the excited state of $_{8}$Be, the analyser needs to separate the data from these two channels. This is done using two different methods. For the first method, the analyser requires the beam energy to calculate the energy cut off for the ground state of $_{8}$Be. Due to the specific nature of the analyser, the beam energy is the only parameter needed for the above calculation illustrated as follows.

Let S_P (18) be the proton separation energy for ^{12}C = 15956.8 keV
Q_α (18) be the Q value of the alpha decay = -7366.57 keV

b be the beam energy

So, the kinetic energy of the first alpha emitted is given as $E_C = (S_P + Q_\alpha + b) \times \left(1 - \frac{M_\alpha}{M_C}\right) + C$ in the centre of mass frame of the reaction, where C is a constant inserted to account for any other energy losses. Now, in the reaction that we are studying, at 2 MeV, this comes out to be roughly 8 MeV. The only particles we can have at this energy in this particular reaction are the alphas.

The analyser calculates the energy and momentum for all the particles. Since the identifier has identified all possible particles and done corresponding energy loss calculations, the analyser selects only the identification where the particle ID is alpha and then looks at its energy. If the energy of the particular alpha is above E_C then it is isolated and added to a 1D histogram, with the theta of this particle on the X-Axis. If it is less than E_C it rejects the particle and moves on. Once the analyser has cycled through all possible hits, we get a histogram which has the distribution of particles as a function of theta. On this histogram, every single particle corresponds to one reaction (since one decay through the ground state gives one alpha particle with this high energy). Hence the total number of events is given simply by total number of particles detected. We can vary parameter C to change the acceptance of events based on inputs from SimX as well as visual inspection of the kinematic curve.

The method above works for alpha particles detected in this energy range. For this to work we need not detect all three particles, but just one. Since each decay emits one alpha particle, this method is easy. Any alpha particles not detected can be attributed to the geometric efficiency of the detection setup. Hence the number of counts can be calculated as a function of angle θ and integrated using the Legendre polynomials to give the total cross section. However, the method above does not utilise the full capability of the setup we have. So, a second method is also employed. In this method, it is a prerequisite that all three particles from the decay must be detected. So, the analyser finds the energy and momentum of all the hits in an event. An event is a time window within which all the hits are collected. So, for a triple alpha decay, an event must have three hits with particle identification as alpha for all three. This is a condition for this method to work. Once we have such a scenario, we select the two lowest energy alpha particles and take their momenta. We calculate the relative momentum $\overrightarrow{p_{2-3}} = \frac{1}{2}(\overrightarrow{p_2} - \overrightarrow{p_3})$ in the centre of mass frame. The total energy of these two particles is given as –

$$E_{Be} = 2\frac{\vec{p}_{2-3}^{\,2}}{2M_\alpha}$$

Equation 2

Now, for the ground state channel, since the first alpha particle carries away most of the energy, the energy available for the unbound ^{8}Be nucleus is very small (of the order of a few keV). So, if the energy E_{Be} is calculated and binned into a histogram, we can see a very sharp peak which can be gated upon. The alphas detected in this region correspond to the ground state of 8Be.

The problem with this method is that it requires the detection of all three alphas. So, even if we miss out on one alpha particle, the method cannot be applied. Since the missing alpha could be any one of the three particles, it is difficult to systematically calculate the efficiency of detection. Moreover, it is difficult to obtain the differential cross section using this method since we have to plot the θ of only the highest energy alpha (since that decays from the compound nucleus). However, a differential cross section plot obtained from such a selection may be incorrect due to undetected lower energy alphas. Further investigations using simulations of the reaction are required to determine exactly how the lack of detection of the lower energy alphas affects the differential cross section.

Theory

Energy loss of charged particles in matter

For the purpose of this study, we need to consider how charged particles can lose energy in matter. Since the events that concern us, solely comprise of alpha particles and protons. We would focus on these two specifically.

The mean rate of energy loss (or stopping power) is given by the Bethe-Block Equation (19):

$$-\frac{dE}{dx} = \frac{4\pi}{m_e c^2}\frac{nz^2}{\beta^2}\left(\frac{e^2}{4\pi\varepsilon_0}\right)^2\left[\frac{1}{2}\ln\frac{2m_e c^2\beta^2\gamma^2}{I} - \beta^2 - \frac{\delta}{2}\right]$$

Equation 3

Where, β and γ are relativistic kinematic variables.

$K = 4\pi N_A r_e^2 m_e c^2$

Z = atomic number of medium

z = atomic number of incident particle

I = mean excitation energy

δ = density effect correction to ionisation energy loss.

The above form of Bethe-Block equation is accurate for moderately relativistic charged particles other than electrons.

In our case, the protons have energies in the range 500 keV to 3500 keV whereas the alpha particles have energy in the range of a few 100 keV to nearly 10 MeV. Clearly, we are operating in the non-relativistic regime and hence, the equation above can be simplified. Since β<<1 , we can take this limit in equation 1 to reduce to –

$$-\frac{dE}{dx} = \frac{4\pi nz^2}{m_e v^2}\left(\frac{e^2}{4\pi\varepsilon_0}\right)^2\ln\frac{2m_e v^2}{I}$$

Equation 4

This is the equation applicable to protons & alpha particles in this study.

At low energy, energy loss therefore varies as v^{-2} reaching a minima at approximately $E = 3mc^2$ where m is the mass of incident particle. For protons this is nearly 3000 MeV. So, in the energy regime we are working in, energy loss decreases with increasing velocity as v^{-2}.

The different corrections to Bethe's formula are not significant in the energy regime we consider. However, energy loss in this study has been calculated using SRIM energy loss tables (20) and they use Bethe's formula with all corrections incorporated.

Now, given the energy loss we can calculate how much distance the charge particle can travel. The particular distance that we are concerned with here is the distance over which a proton and an alpha would deposit all its energy in silicon, since the detectors are silicon detectors.

The range of the particle can be determined by integrating equation 1 over E with limits 0 to E_0, where E_0 is incident energy of particle.

Using the SRIM tables (20), it can be shown that protons of 3500 keV can travel nearly 120 μs in Silicon, while alpha particles of 10 MeV can travel only 70 μs. While these calculations are based on SRIM tables, due to large number of particles, not all particles will have the same distance. Hence,

the range experimentally observed is not a delta function but a Gaussian around the calculated value. This is due to the statistical nature of energy loss. The small variations in the number of collisions required to bring a particle to rest give rise to the variation in range, called straggling.

Resonances in Nuclei

A good question to ask right now would be "What is a resonance?"

Where there are several different ways one could approach the question, in this section I would begin with how resonances are seen in scattering cross section followed by a brief outline of theoretical framework that would explain said observations (21).

Experimentally, the occurrence of a resonance is seen when the cross section of a reaction is measured as function of energy of the incident particle. It is seen that for certain values of energy, the reaction rate is enhanced. However, this peak in the reaction cross section can exhibit significant variations in terms of the height. (Quantifying how much the reaction is enhanced) and the width.

It is generally observed that the widths of resonances increase with increasing energies. At high energies, the width of a resonance may exceed resonance separations and then no resonance can be observed. The objective of this section is to qualitatively explain the concept of resonance.

Consider a nuclear reaction where an incident particle bombards on a target. In the first step, this leads to the formation of a compound nucleus. Subsequently, this compound nucleus, after a long time (on nuclear timescales), decays into the final nucleus and secondary particle. The occurrence of a resonance can be explained as follows.

The compound nucleus has definite states s of energy E_s. If ε is the energy of the bombarding particle and B is the binding energy of the target nucleus, excitation energy of the compound nucleus is given as $E = \varepsilon + B$. So, a compound nucleus only forms if $\varepsilon = \varepsilon_S$. These states have a definite lifetime τ_s (since they decay) and by extension, the energy E_s has an associated width Γ_s given by –

$$\Gamma_S = \frac{h}{\tau_S}$$

Equation 5

One may question why the excited nucleus has discrete quantum states by drawing an analogy with an atom where an incident particle has energy above ionisation energy. The excitation energy of a compound nucleus is always greater than B, so we should expect a continuous spectrum.

To understand the above, we recognise that the nucleus is a fundamentally different system as compared to an atom. It has the following properties, taken as assumptions (based on experimental evidence) –

i. The nucleus has a well-defined surface, which is a sphere of radius R. If the distance of a particle from the centre of the nucleus is greater than R, no nuclear forces act on the particle.

ii. If the particle penetrates the nuclear surface, it moves with an average kinetic energy ε_{IN} which is very large compared to energy outside the nucleus.

iii. The particle a is subject to very strong interactions inside the nucleus so that it interchanges its energy rapidly with the other nucleons.

Now consider an incoming particle. The nuclear surface is essentially a barrier. This can be understood by considering assumptions 1 and 2. The wavefunction outside the nucleus has an

associated wavenumber k. On passing through the barrier, this changes to K with K > k. The ratio of penetrating particles to incident particles is given as –

$$P = \frac{4kK}{(k+K)^2}$$

Equation 6

Thus the surface offers obstruction to any incoming particle which is nearly 100% for k << K.

While there can be a quantitative and rigorous treatment of resonances in a nucleus, the description provided here is rather elementary. However, it conveys important physics which we would like to understand.

Consider a nucleus which has energy levels which have a level distance D. While the motion of nucleons cannot be described by a classical picture per se, we can still make a connection by making use of the correspondence principle. According to the principle, the states which are highly excited correspond more readily to a classical system. If one builds a linear combination of wavefunctions describing the nucleons inside the nucleus, one would get a picture which localises the particles relatively well, within the constraints imposed by the uncertainty principle. What we wish to ultimately be able to explain within the framework are the widths of the resonances and their properties. For this purpose, let us assume that the period T, after which the initial grouping of the particles reoccurs. Let us assume that energy levels are spaced equally $E_n = E_0 + n\Delta$ and E_0 is the level spacing in this scheme. Clearly, the wavefunction Ψ for this nuclear system is given as –

$$\Psi = \sum_{n=1}^{N} a_n \varphi_n \exp -\frac{iE_n t}{\hbar} = \exp -\frac{iE_0 t}{\hbar} \sum_{n=1}^{N} a_n \varphi_n \exp -\frac{in\Delta t}{\hbar}$$

Equation 7

From this equation, we can clearly see that $\left|\Psi\left(t + \frac{2\pi\hbar}{\Delta}\right)\right| = |\Psi(t)|$ so that the wavefunction Ψ repeats the configuration after time $t = \frac{2\pi\hbar}{\Delta}$. Thus, the period of the motion in this case becomes –

$$T = \frac{2\pi\hbar}{D}$$

Equation 8

Now, in complicated systems, where level spacing is no longer uniform, we may not have such a time period T, but the average level spacing D can be considered instead which can be an indication of the period of nuclear motion.

Now, due to the reflection a nucleon undergoes while attempting to enter or leave a nuclear potential well, the particles inside undergo reflections which give rise to periodic motion. While one would intuitively think that above excitation energy this periodicity should cease, such reflections essentially ensure that the motion above excitation energy is similar to the one below it. This periodicity in motion gives rise to an energy quantisation and to the existence of discrete states. These states are not strictly stationary due to the possibility of nuclear fission.

Consider a level with width Γ_a, placed s above binding energy B from which emission of a particle a is possible. Now, if this level was generated from a configuration where particle a was just entering the nucleus, it should also be able to leave through the same configuration. The time period taken for the nucleus to return to this initial configuration is given by T which is of the order of $\sim \frac{2\pi\hbar}{D}$

where D is again, the average level distance. However, the reoccurrence of the level does not necessarily entail a decay. If that were the case, the lifetime of the level τ would be comparable to T and width $\Gamma_a = \hbar/\tau$ would be of the order D. But we know this is not the case. In fact, for a well-defined resonance, $\Gamma_a \ll D$. Thus, the lifetime of the state is actually much longer than the time it takes for the system to come back to its initial configuration. This implies a picture where the particle a is returning again and again to its initial configuration and "knocking" on the door with probability P_a being the penetrability of the surface. Thus, the width becomes –

$$\Gamma_a \cong P_a \frac{D}{2\pi}$$

Equation 9

Now, if an incident particle has low energy, the widths of resonances are small due to the following factors –

a. The strong interactions between nucleons – This results in a long period of nuclear motion, which results in small values of D.
b. The small penetrability factors of the nuclear surface – This results in the lifetime of the compound state much longer than the period, which results in a small width.

These two factors combine to make the width of the level small as compared to D and establish the possibility of resonances.

Cross Section

We wish to measure the cross section for the reaction ^{11}B(p,α)2α. In this section, I would briefly outline some experimental aspects of measuring a cross section.

Let N_{INC} = Number of incident (beam) particles.
N_{EV} = Number of events (beam – target interactions)
n = Target atoms per unit volume = $\frac{\rho N_A}{A}$
A = mass number of target (assuming a single pure isotope)
ρ = mass density of target (g/cc)
ρx = areal density of target (g/cm$_2$)
nx = areal number density (atoms/cm$_2$) = $\frac{\rho x N_A}{A}$

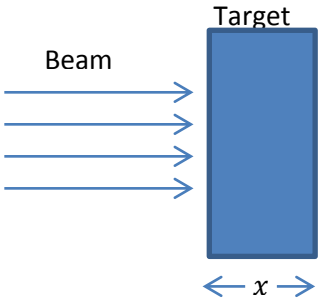

Figure 5 - Beam Target Interaction

Now, probability of interaction depends on the properties of the beam and target particles. If we have a thin target, then we can consider the following scaling relations –

i. Number of interactions is proportional to number of incident particles

ii. Number of interactions is proportional to thickness x of target

iii. Number of interactions is proportional to density ρ of target

$$N_{events} = Constant \times N_{inc}\, nx\, \sigma$$

We set the constant = 1 to get –

$$N_e = N_{inc}\, nx\, \sigma = N_{inc} \frac{\rho x N_A}{A} \sigma$$

Equation 10

The strength parameter σ is given the name cross section for the reaction. This naming, which may be attributed to dimensions of the parameter (area) has a historical context. Historically, scattering was understood classically as a collision between two objects. In that context, the cross section was the area of the target which an incident particle could hit and interact with.

So, the cross section is defined as –

$$\sigma = \frac{N_{events}}{N_{inc}\, nx} = \frac{N_{events}\, A}{N_{inc}\, \rho x\, N_A}$$

Equation 11

The expression above holds true if we can detect particle flux in the entire 4π solid angle sphere. However, from an experimental point of view, that is seldom the case.

A typical detection setup has a detector whose solid angle is given as dΩ. In such a case, we can only detect counts in this dΩ out of the total solid angle of 4π. So, we define the quantity differential cross section as –

$$N_{events\ in\ solid\ angle\ d\Omega} = N_{inc}\, nx \left(\frac{d\sigma}{d\Omega}\right) \Delta\Omega$$

$$\frac{d\sigma}{d\Omega} = \frac{N_{events}}{N_{inc}\, \Delta\Omega\, nx} = \frac{N_{events}\, A}{N_{inc}\, \Delta\Omega\, \rho x\, N_A}$$

Equation 12

In the case of this specific experiment, N_{inc} is calculated by measuring the total charge deposited by the beam into the Faraday cup, and dividing it by the charge of the incident particle, which in this case is a proton. This gives the final relation as –

$$\frac{d\sigma}{d\Omega} = \frac{N_e A e}{Q\, \rho x\, N_A\, \Delta\Omega}$$

Equation 13

Coulomb Barrier

In the case of the reaction we wish to study. The incident particle is a proton and the target is a ^{11}B nucleus. Instinctively, we can understand that a nuclear reaction can only take place if the incident particle and target are close enough for nuclear forces to play a part. Thus, the incident particle must have sufficient energy to overcome the Coulomb barrier. The energy required for a particle of charge z is to overcome Coulomb barrier for a target ${}^{A}_{Z}X$ is –

$$E_C = \frac{1}{4\pi\varepsilon_0}\frac{zZe^2}{r}$$

Equation 14

Where the radius r is the channel radius for the reaction and can be approximated as $r = \left[A_X^{\frac{1}{3}} + A_Y^{\frac{1}{3}}\right]$ where r_0 = 1.4 fm. For z = 1, Z = 5, A_X = 11 and A_Y = 1, r ≈ 3.62 fm, which gives E_C ≈ 2 MeV. So, we shouldn't see any reactions below this energy in the classical physics domain.

However, since we are in the quantum physics domain, there is always the possibility of tunnelling which gives the resonances below this energy.

Conservation Laws in Alpha Decay

The conservation of angular momentum, in addition to energy and momentum, is essential to explain the resonances seen in α-decay of the compound nucleus. Although the selection rules are well understood, they are briefly described here with special reference to α-decay (22).

In any α-decay, one of the decay products is an alpha particle. This results in a special set of constraints on the reaction. The nucleus can decay from an initial state I_i with angular momentum to a final state I_f. The angular momentum of α particle can thus range from $I_i + I_f$ to $|I_i - I_f|$. However, an alpha particle has two protons and neutrons with spins coupled pairwise to 0. So, intrinsic spin of an α particle is 0 and entire angular momentum carried away must be orbital in nature. Let this be l_α. Since the wave function is a spherical harmonic Y_{lm} with $l = l_\alpha$, a parity change of $(-1)^{l_\alpha}$ is associated with the decay. This gives us the parity selection rule, indicating which transitions are permitted and which are absolutely forbidden by conservation of parity. If the initial and final parities are the same, then l_α must be even; if the parities are different, then l_α must be odd. Let us consider the effect this has on the states of ^{12}C. The relevant resonances are described in Table 1 (2) –

E_P (MeV)	$\Gamma_{C.M.}$ (keV)	$\Gamma_{\alpha 0}$ (keV)	$\Gamma_{\alpha 1}$ (keV)	Γ_P (keV)	$^{12}C^*$ (MeV)	Jπ; T
0.162	5.3 ± 0.2	0.290 ± 0.045	6.3 ± 0.5	0.0217 ± 0.0018	16.1058 ± 0.0007	2^+ ; 1
0.675	300	< 0.27	150	150	16.576	2^- ; 1
2.00	96 ± 5	4.6	11.4	76	17.79	0^+ ; 1
2.66	400	65	177	68	18.38	3^- ; 1
3.5	1100	50	200	300	19.2	(1^- ; 1)

Table 1 – Known Resonances in ^{12}C for ^{11}B(p,α)2α reaction

We can compare this to the ^{8}Be whose ground state has a width of 5.57 ± 25 eV (18) with J^π of 0^+ with T=0 whereas the excited state at 3030 ± 10 keV with a width of 1513 ± 15 keV is a 2^+ state with T=0. We can see that among the resonances in ^{12}C which can be seen in this experiment, only the one at 675 keV is an unnatural resonance. Thus, we don't see a decay from this state to the 0^+ ground state of ^{8}Be. This is an example of a selection rule resulting in an absolutely forbidden decay.

Calibration

The detection system can only provide us with voltage values which are proportional to the total energy of the detected particle. To find out the actual energy, we need to calibrate the detectors with a source of known energy. However, the experiment here is slightly more complicated than a simple energy calibration. In addition to energy calibration, we also need to calibrate the geometry of the setup. This is because we are trying to calculate the momenta as well as the energy of the particle. The geometry of the setup is essential since we want to do dead layer corrections in the target as well as the detectors in addition to the energy loss calculations. Even for the energy loss calculations, we assume a point as the origin of the decay (which is roughly speaking, the beam spot) and from this point we calculate the velocity vector of the alpha particle detected by finding the vector in direction of the pixel in which the particle was detected. These calculations require a precise knowledge of the geometry of the system. Thus, a calibration is required.

In this chapter, I would briefly describe the energy and geometry calibrations, how they were carried out, present examples of a few technical difficulties encountered along the way and the steps taken to resolve them.

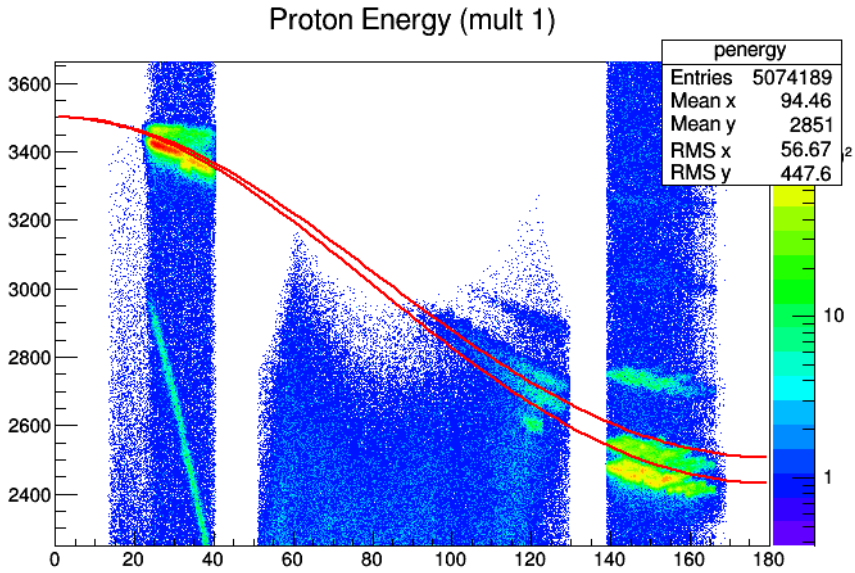

Graph 1 - Kinematic Curve obtained at incident proton energy = 3500 keV

Two tools helped us to see if the calibration was correct or not. The first of these was a kinematic curve, which was plotted at the end of the analysis. The second was a ROOT macro (23), KinCur, which was used to generate expected kinematic curve for scattering of particles. To appreciate the tricky nature of the problem, I am briefly outlining chronologically the calibration curves and the corrections made to the same.

The kinematic curve is essentially an Energy vs. Theta 2D histogram. The two lines seen above in the kinematic curve are the output of the ROOT macro used to overlay a kinematic curve which is expected for the given reaction. The two streaks that we can see correspond to expected elastic scattering of protons off ^{11}B and ^{12}C. Note that this ^{12}C is not the Carbon formed as the compound nucleus in the reaction but in the Carbon backing on which the Boron foil is placed. A reference to

figure 2 would explain the blanks around the 45° and 150° marks. This is the region where we don't have a detector and hence are expectedly blank.

Initially we had ruler measurements and an old calibration done quite a while ago, to guide us. This gave the kinematic curve Graph 1. This was essentially the starting point of both the energy as well as geometry calibrations. Before proceeding to discussion specifically on Geometry and Energy calibrations, I would briefly like to take a pause to describe the salient features of the above Kinematic Curve. These features provide great insight into the detection setup as well as methods of analysis employed in the experiment.

The theta region from 20° to 40° corresponds to the downstream S3 detector (labelled SD for the remainder of the report for convenience). The region from 50° to 130° corresponds to both W1 square DSSDs (Labelled Det1 and Det2 for the remainder of report for convenience). Finally, the remaining region from theta 140° to 170° corresponds to the upstream S3 detector (labelled SU for the rest of the report). The terms 'upstream' and 'downstream' may also be used in the report and correspond to direction with respect to beam. Downstream implies in the direction of beam from the target whereas upstream implies opposite to the direction of beam from the target.

Having described the different detectors and their outputs as seen on the kinematic curve, we now proceed to features of the curve itself. The most prominent feature is the lack of data in Det1 and Det2 in the region above 3 MeV approximately. This is due to the thickness of the detector. Det1 and Det2 had thickness of 60 μm whereas SU has a thickness of 322 μm and SD 1038 μm. The thickness sets a limit on how much energy can be deposited in the detector for a proton and an alpha. This will be useful later as we can be sure that any particle detected in Det1 and Det2 above this energy is an alpha particle and not a proton. Also notice that this region has symmetry about the centre with peaks towards the end points. This is because of the geometry of the setup. The particle travels the least distance through the detector near the centre. However, as one measures further away, the effective thickness of the detector increases, hence more energy can be deposited in the detector.

A careful inspection of the kinematic curve shows that several different of these streaks originate from the red spot in the SD. The reason why all streaks originate from this point is because this corresponds to the beam energy for this kinematic curve at low scattering angles. The expected energy loss is minimal for low angles and hence most streaks do not lose too much energy and are clustered in a compact manner as seen above. As the angle increases however, we see that these streaks start to diverge. Typically, if the target has higher mass, the incident particle will carry away a greater portion of the energy even after scattering and hence, the streak will lie higher for a higher mass at large angles.

Now, if we look at the kinematic curve again, we can see other streaks in the SU. These have been tentatively identified as Oxygen, Aluminium and Copper after the Carbon streak. These streaks are seen for the following reason. Oxygen is seen since the sample prepared is a natural boron sample and water cannot be completely eliminated from it. The sample preparation was carried out in a cauldron whose base had copper content which has contributes a minor impurity in the sample (24). The exact source of the aluminium impurity cannot be traced but can be attributed to sample preparation.

A final rather steep streak can be seen only in the SD. This is the proton-proton scattering and is expected in the curve.

Geometry Calibration

As previously mentioned, the target is surrounded by two W1 and two S3 detectors. The purpose of doing geometry calibration is to find the exact positions of these detectors with respect to a fixed origin. The position of the detector is characterised by three sets of coordinates which are the position, normal and orientation. These are calculated with respect to the origin which is taken to be the beam spot. Calibration of the geometry proved to be trickier than previously anticipated.

To calibrate the geometry, a source of thickness ≈ 3 mm was placed facing the detector inside the chamber. This run was then recorded. From the data from this run and previously existing energy calibration, a hit pattern of the run was recorded. This hit pattern was then used to calibrate the geometry using a GeoDWIM fitter.

GeoDWIM stands for Geometry Do What I Mean fitter. It uses a combination of isotropic and a polynomial fitter. An isotropic fitter assumes that the source is isotropic in its radiation and the number of counts in a pixel is proportional to its solid angle. It may be a point source or an extended source. It then locates the point in the hit pattern which has the highest number of counts and then calculates the origin of the source based on the hit pattern. On the other hand, a polynomial fitter tries to find where the Number of counts in a pixel vs. distance from the source has least amount of deviations among the points by fitting a 4^{th} order polynomial to the data. However, this method is not sensitive to the distance along the normal. The GeoDWIM is a part of the AUSAlib toolbox (25).

The combination of the two methods above should work just fine to give a good geometry calibration. The problem is that the source itself has a thickness of 3 mm which cannot be taken into account by using these methods. Thus, when considering data from the beam, one has to adjust the geometry calibration to make sure the kinematic curve fits right.

On the surface, it looks fairly simple. One should obtain the calibration of individual detectors using GeoDWIM and then add 3 mm along the normal to get the geometry of the system. However, since we require the geometry to calculate dead layer energy losses, etc… accuracy up to the order of nm is required of the setup geometry. This cannot be obtained by arbitrary addition of 3 mm (measured using a Vernier Callipers).

To avoid this problem, a different geometry calibration tool was devised by Michael Munch called the RutherFitter. As the name suggests, the RutherFitter uses the data obtained not from a source, but from the Rutherford scattering of a beam. This is an important improvement over the GeoDWIM in a significant way. Since the RutherFitter utilizes the data from a beam, we no longer have to modify the geometry calibration from a source. We can directly use the geometry obtained from the beam data. Compared to the GeoDWIM, however, the RutherFitter has its own drawbacks. Since the target was mounted on the ladder, the shadowing from the ladder causes significant calibration issues. The run used to calibrate using RutherFitter was alpha particles bombarding on a Gold foil.

The RutherFitter was originally programmed to fit one detector at a time. However, it was found that fitting one detector at a time caused problems since the program had a heavy correlation between z direction and A which is the angle of the target. This means that the program fitting

routine gives similar results whether we change the z direction (beam direction) or the angle of the detector.

Eventually, after a lot of troubleshooting, this problem was identified and RutherFitter was modified to fit multiple detectors at a time. Once this was done, I used RutherFitter to fit all 4 detectors at once. Before looking at the results from RutherFitter, I would like to show what a typical hit pattern looks like. This is shown below and described thereafter.

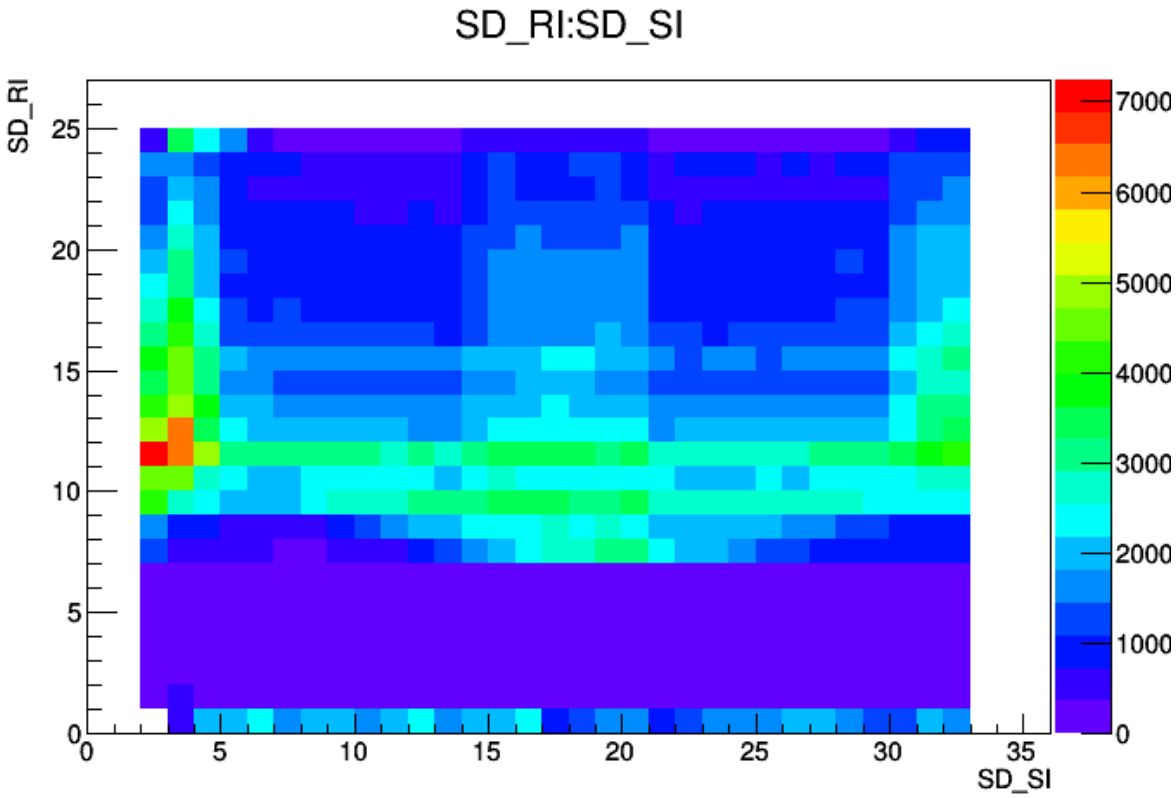

Figure 6 - Hit Pattern for SD at 2000 keV

Figure 6 shows the Hit pattern for SD at 2000 keV. The plot is the number of hits on the rings vs. the number of hits on the spokes. As previously mentioned, there are 24 rings and 32 spokes. The hits are plotted on the Z-Axis. This is a typical example of a good, flat beam. We want a beam that is centred on the target. This means that the distribution along the spokes should be even. Secondly, we don't want a beam that is shifted to the left or right. A beam shifted to the left would show high number of counts around spoke 16 (towards the centre). One shifted to the right would show high counts around spokes 0 and 32 (towards the sides). We don't see anything in the lower rings because this area is shadowed by the target and prevents too many beam particles from being incident on it. This snapshot was taken during a run. As a result, there are these gaps present in the centre of this band and large incident hits towards the edges for large ring numbers (around Spokes 0 and 32). This is due to the downscaling trigger. We downscale the acceptance by a factor of 8, i.e. we select every 8^{th} event in the downstream. This is because of the large number of events incident on the SD. However, we still need these events for an overall normalisation.

Having understood how the SD hit pattern looks, we can now easily understand how the hit patterns for SU, Det1 and Det2 look. The plot is essentially a 2D histogram of number of front strip hits vs.

number of back strip hits. Now, we are ready to take a look at the results from the geometry calibration using RutherFitter. The results of this fit are shown below –

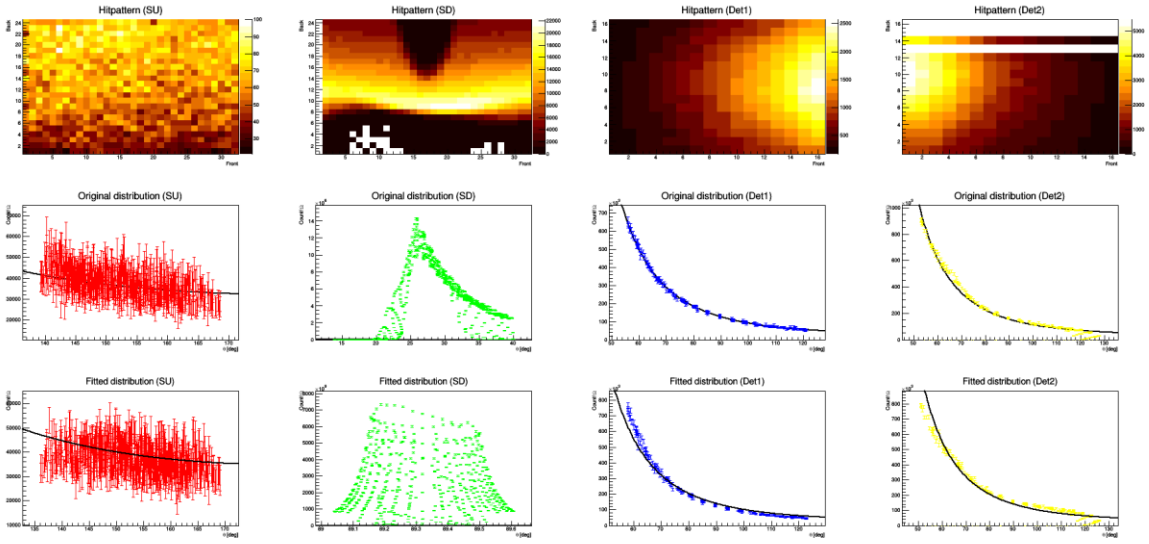

Figure 7 - RutherFitter Output for all 4 detectors

The plot can be understood as follows. The four detectors are arranged in 4 columns (From left to right – SU, SD, Det1 & Det2) with three rows of plots. The first row is the hit pattern on the detector. The second row is the original distribution. The third row is the distribution after geometry fitting was applied. One can immediately spot the problem. Firstly, the downstream detector hit pattern has shadowing which gives a rather strange looking skewed fit. Secondly, the lack of statistics in the upstream detector gives large error bars. The geometry obtained from this run was so far off the ruler measurements (which can have an error bar of ± 2 mm at the most) that this run had to be immediately discarded.

RutherFitter is a versatile tool and has several options. Faced with the above problems, we decided to flex its muscles. Due to the difference in statistics in SD and SU, we decided to fit simply SD with either Det1 or Det2 since they are perpendicular (and eliminate the problem of Z-Axis and angle correlation). Once we fit this, we locked these two detectors into place and fitted all four together with the positions of the previously fitted detectors locked. This still didn't solve the problem due to the low statistics.

To counter the problem of shadowing, it was decided to simply disable the shadowed strips. By disabling the strips, it is implied that in the process of front back matching (at the Sorter step), these strips were considered non-functional and hence no data was taken. Having disabled the strips would mean that there was no data in this region (akin to a region where there is no detector) and we hoped this would fit better. The results of this fit are shown below –

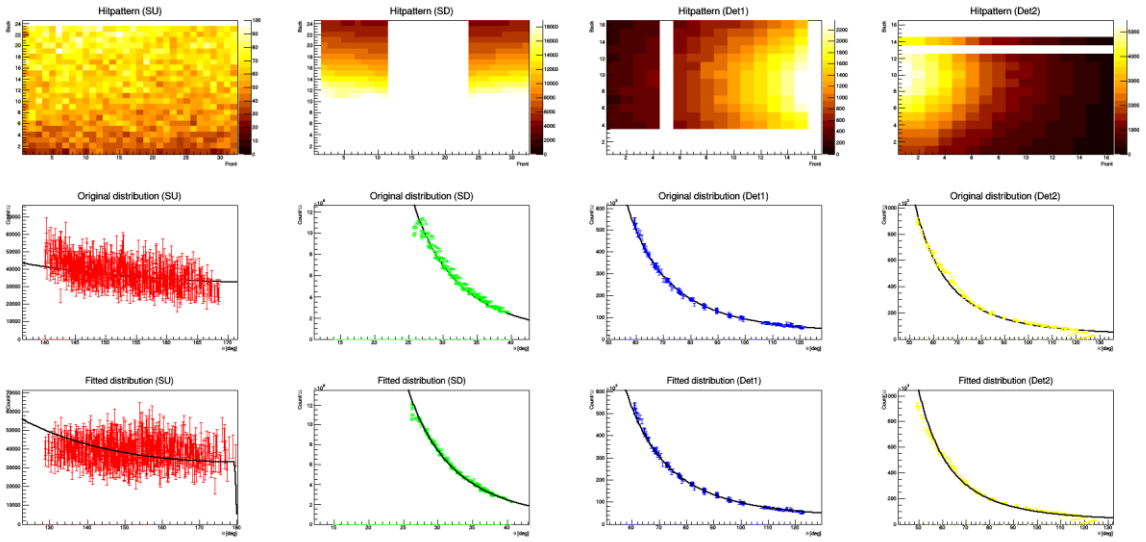

Figure 8 - RutherFitter output after disabling shadowed strips.

The figure shows a much better fit for SD, Det1 and Det2 whereas the SU is still suffering from the lack of statistics. However, once again, on comparing the results of this fit to the data taken by rulers, it was found that the fit couldn't be right. So, what were we missing?

Eventually we figured out the problem. The programming of the RutherFitter assumes that there is only one constituent in the sample. If we look back at the kinematic curve in Graph 1, we can immediately spot the problem. The Gold foil target was deposited on a Carbon backing. This carbon backing had its own streak of Rutherford scattering. While the fitter could distinguish between the two streaks in Det1, Det2 and SU (despite the lack of statistics), this was not the case in SD, which was the root cause of the problem.

So now the problem was to separate the track due to gold from the one due to carbon and then apply the RutherFitter. Unfortunately, despite our best efforts, we could not solve this issue and eventually, due to temporal constraints, had to move on to other methods to calibrate geometry.

The other method was the GeoDWIM method as previously mentioned. But we had to find a way to make the uncertainty due to source thickness go away. So the following strategy was devised for the same purpose. Firstly, individual detectors were all calibrated using GeoDWIM. After this was done, a distance of 3 mm was added arbitrarily to all the calculated values. Once this was done, the data for the $^{11}B(p,\alpha)2\alpha$ run at 2000 keV was taken. On this run, the proton scattering track on ^{11}B was considered. Now, we plot the track due to protons scattering off ^{11}B and ^{12}C using the ROOT macro. Then we observe the graph and observe if the curves match. One important caveat here is that since the ROOT macro gives the energy in the lab frame without any energy loss in the target or dead layers, this observation has to be done after the entire analysis has been done and all energy loss corrections have been carried out. Needless to say, such a calibration is a time consuming task since energy loss corrections along with all the changes in detection settings take some time to carry out. Moreover, this is not fitted using a computer, but manual fitting, so every correction need not take us closer to our goal. To explain exactly how the change in geometry affects the kinematic curve, we take a look at one of the curves from an early attempt at this method.

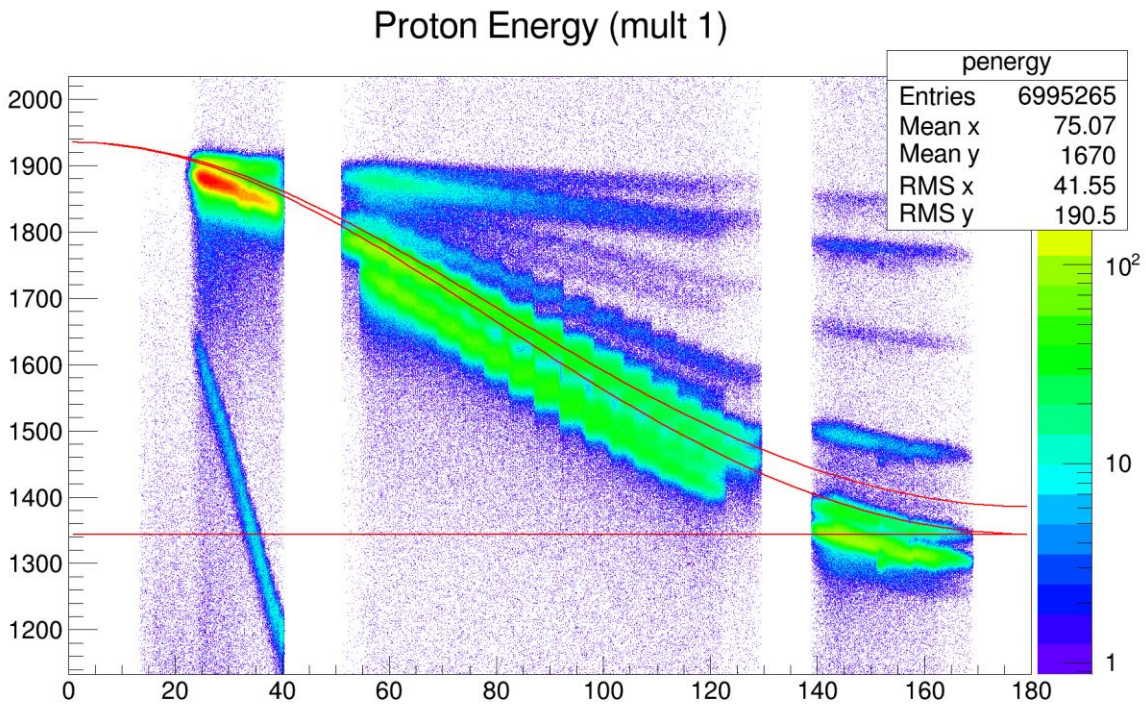

Graph 2 - Kinematic Curve at E = 1935 keV

As mentioned previously, this kinematic curve has been obtained after the analysis was completed. It is quite clear from the graph that the tracks do not match the kinematic curve from the data and the data is underestimated. For now, the accuracy of the histogram need not concern us. What we wish to understand is how the curve changes as the geometry of the setup changes.

Consider the range for the W1 detectors Det1 and Det2. In this kinematic curve, we can clearly see a new track appear close to 55° and end close to 120°. This clearly shows that while Det1 and Det2 are placed on either side of the target, their location is not exactly symmetric and they cover different angular range. The detector which is closer will have a larger angular range. So, increasing the distance of the detector from the origin has the effect of shrinking this histogram horizontally about the centre of the detectors. We need to understand how the detector is defined in the setup to understand exactly what can be changed and how it will affect the graph. The only vector we can really change is the position vector. As things are currently defined, the position vector is specified in Cartesian coordinates. If we transform it into polar coordinates and increase the radius, it has the effect of shrinking the graph horizontally about the vector. To change the angular range, we can vary the angle θ of the detector. So, when we are carrying out calibration, if the kinematic curve is overestimating energy at the end of energy loss corrections only slightly, we can increase the value of theta to move the detector to the right on the kinematic curve which would have the effect of decreasing the difference in kinematic curve and the ROOT macro projection.

The effect of such variations in the S3s is not quite the same. For a start, being an annular detector, bringing S3 closer to the target will not indefinitely increase the solid angle coverage on the kinematic plot (i.e. result in horizontal stretching) but will increase to a maximum and start decreasing again. This has the effect of making the angular range being more or less fixed for the S3

detectors. As a result, their geometry cannot be manipulated as much as the W1s, but the concepts are still the same as before.

So, having described how the variation in geometry manifests itself on the kinematic curve, we are in a position to discuss the results of this geometric calibration. The graph plotted after completing geometry calibration is presented below –

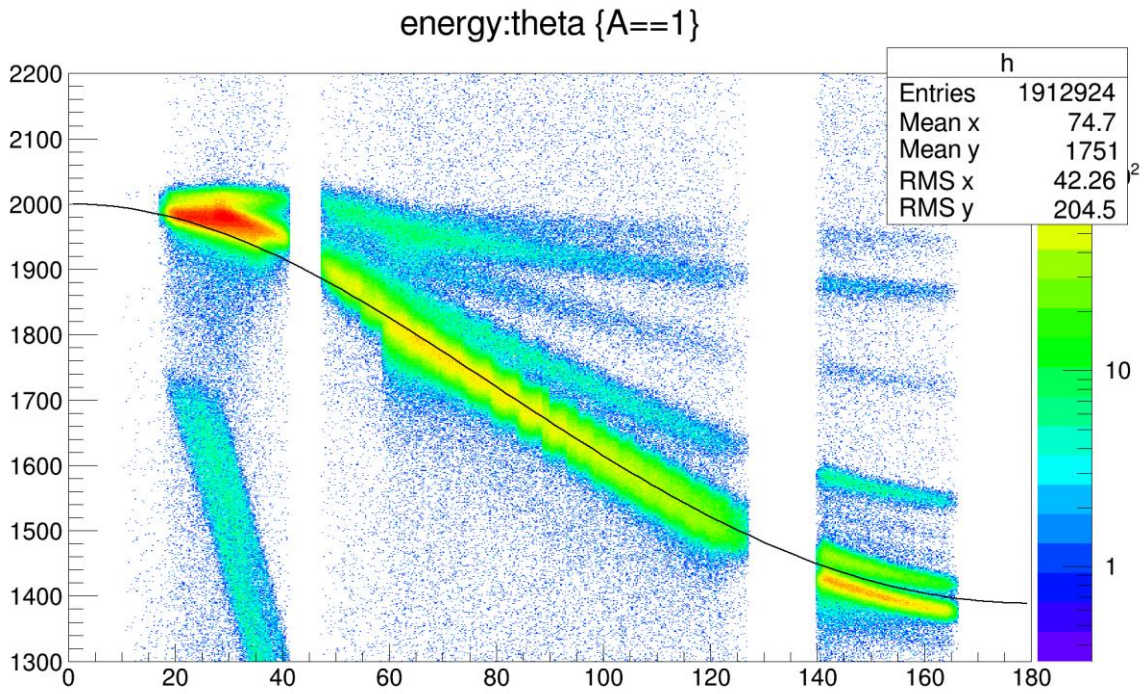

Graph 3 - Kinematic Curve for Geometry Calibration at 2000 keV

As can be seen from the above plot, while Det1 and Det2 appear to be fairly well aligned, there are still problems with SU and SD. The energy difference however, at the most was about 20 keV for SD and SU. This was taken to be an acceptable result and this geometry was used for further calibration for energy. The only lingering doubt was that the SD data was higher than the macro which was a cause of concern since energy corrections were fairly accurate and should by no means exceed the expected curve.

However, this was not the final geometry calibration. I would return to this towards the end of this chapter.

Energy Calibration

This is the traditional calibration that is expected in a detector setup. For the purpose of calibration, we used a source with known values of peaks and calibrated individual detectors accordingly. For this purpose, each strip on all 4 detectors has to be individually calibrated. In sharp contrast with geometry calibration, this sounds harder than it actually was. Thanks to a graphical tool created by Jesper, energy calibration could be carried out with ease strip by strip with careful inspection of residuals after fitting peaks to them.

At this point I must take a pause and admire the work done by Hans, Jesper, Michael and Oliver in building AUSAlib from the ground up. It is an impressive array of tools which can do almost anything you would need to do given the experimental setup and requirements.

So, coming back to geometry fitting, a triple alpha source was used for the energy calibration. The energy peaks used are tabulated as follows –

Element Isotope	I_α (%)	Peak Energy (keV)
^{241}Am		3182.690
^{239}Pu	73.3 (8)%	5156.59 (14)
^{244}Cm	76.4 (12)%	5804.77 (5)

Table 2 - Energy peaks used for Energy Calibration

The peak fitting should, in principle, not be too complicated. However, the asymmetric response of silicon detectors has been well known for some time now. As a result, instead of fitting a Gaussian peak, as should be the case, we fit a Gaussian function folded with a single left handed exponential tail. This fitting function is of the form (26) –

$$f(E) = \frac{A}{2\tau}\exp\left(\frac{E-\mu}{\tau}+\frac{\sigma^2}{2\tau^2}\right) erfc\left[\frac{1}{\sqrt{2}}\left(\frac{E-\mu}{\tau}+\frac{\sigma}{\tau}\right)\right]$$

Equation 15

Where, A is the peak area,

μ is the formal peak position,

τ is the tail parameter, and

σ is the width of the Gaussian component

Even though the peaks all appear in doublets, we have carried out the fit with respect to a single component which has the dominant contribution.

At this point, we can step back and examine the calibration with respect to the experiment that we are trying to do. As we can see, the three data points are approximately at 3.18 MeV, 5.1 MeV and 5.8 MeV. However, in the experiment we are performing, the energy of the scattering protons can be as low as 500 keV, whereas the energy of the most energetic alpha particles can be as high as 10 MeV. So, the response of the Silicon detector needs to be examined and its linearity needs to be verified.

Having performed the energy calibration, we need to now understand a few subtle points which were key to obtaining the final calibration, both in terms of energy as well as geometry. For this, we need to take a closer look at the process of calibration.

The energy calibration was done using a triple alpha source which emits at three known energies. However, the channel at which the peak appears cannot be directly assigned the energy value of the peak. This is because we have to take into account the energy loss of alpha particles in the dead layers of the detectors. This is the part of calibration where energy and geometry calibrations are subtly linked together.

Consider this. To perform the energy calibration, we need to calculate the energy loss of alpha particles in the dead layers of the detector. For this, we require an accurate geometry calibration. But as we saw previously, the geometry calibration was done by manually adjusting the kinematic curve after all energy loss corrections were done. This should not be problematic in principle. But there is another subtle point we need to consider. When we consider the energy loss at the time of calibration, we take into account the dead layer of the detector. Now, assume that this dead layer entered is wrong. Then, at the time of energy calibration, the energy by which the peak is shifted is the energy the alpha particles have lost in the dead layer. This energy is assigned to the channel. However, when we are looking at the elastic scattering of protons and carrying out energy loss correction, the energy a PROTON would lose in the same thickness of dead layer is added in the calculation! So, an incorrect value of dead layer would give an incorrect kinematic curve. For example, assume that the dead layer is overestimated by 100 nm, then, at the time of calibration, the peak is shifted in energy by the amount an alpha particle would lose in 100 nm of silicon. However, at the time of energy loss corrections, the energy added back is only how much a proton would lose in 100 nm of silicon.

Hence, an **OVERESTIMATION** of dead layer would give an **UNDERESTIMATION** of proton energy after energy loss corrections have been carried out and vice versa.

Now, we can look back at the kinematic curve obtained at the end of geometry calibration in Graph 3. The elastic scattering track looks strange both for the SD as well as the SU. So, as a final measure to confirm the geometry as well as energy calibration, we consider the following. We know that the reaction $^{11}B(p,\alpha)2\alpha$ decays to the ground state of ^{8}Be. This ground state is characterised by an unbound state of very small width, which has the following effect; most of the energy is carried away by the alpha particle emitted first. This energy is of the order of 8 MeV at 2 MeV beam energy. In addition to this, since the excited state of ^{8}Be lies approximately 3 MeV with a width of 1.5 MeV, the elastic scattering track of the highest energy alpha particle from the ground state of ^{8}Be is very clean and can be easily identified. The idea is to use this track to calibrate geometry manually as was done for protons previously. The advantage here is that even if the dead layer estimation is wrong, since we are calibrating with alphas, any energy subtracted at the time of energy calibration would be simply added back at the time of energy loss corrections. Thus, this method is not sensitive to an error in dead layer estimation. Once geometry has been established using this method, we can use that confidently to confirm the energy calibration (particularly, the dead layer can be varied so that the proton track also matches the expected kinematic curve). The final dead layer used was based on calculations carried out independently by Michael Munch.

Once this idea was devised, the execution was fairly simple. The methodology was identical to that which was used when calibrating using scattered protons. The final kinematic curve obtained along with the expected kinematic curve is shown in Graph 4.

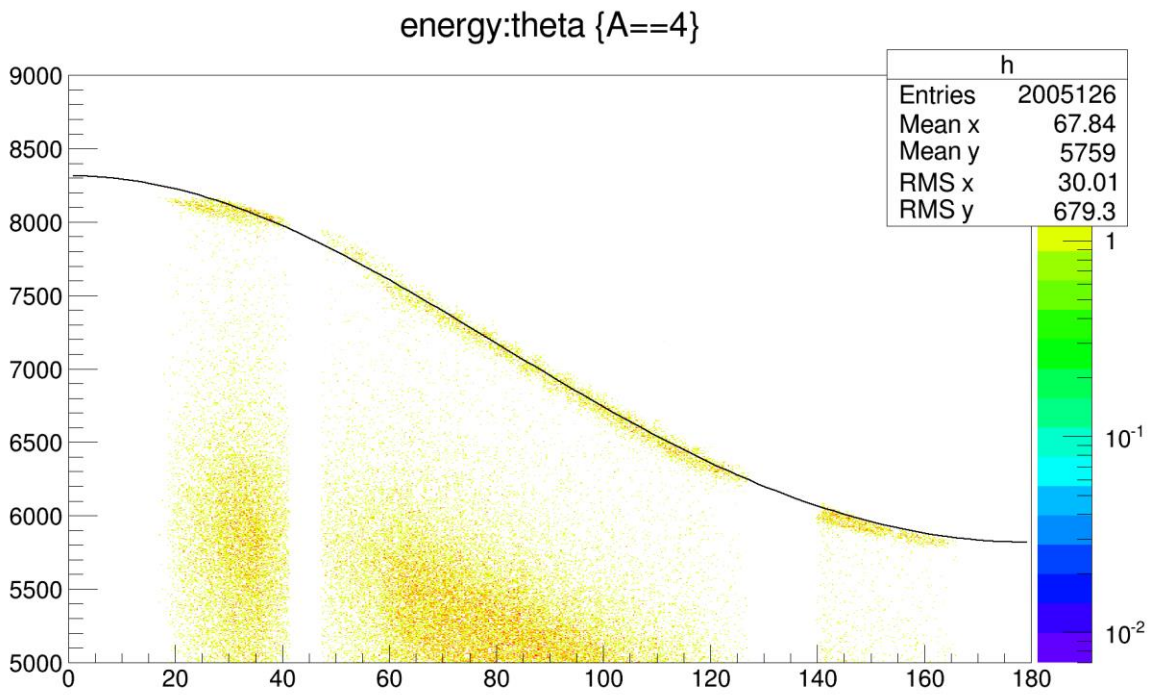

Graph 4 - Kinematic Curve at E = 2000 keV using alpha particles from ground state channel of ^{8}Be. Maximum difference from the expected curve is approximately 35 - 40 keV which was deemed acceptable for an alpha particle.

So, finally, after a long, slow deliberate process of calibration, where we had to consider very subtle details and remote possibilities, we arrived at this geometry calibration. I can say with confidence that we systematically considered all different possibilities, eliminated as many sources of error as we could before arriving on the consensus that the geometry under consideration is the true geometry of the setup. At the risk of sounding philosophical, I would conclude this lengthy chapter by mentioning that it was a long, arduous task, but the journey made me understand the setup, electronics as well as the analysis framework much better than I could have by just studying from a book.

Data Analysis

Having completed the calibration, we now move on to analysis of the data. This is the penultimate step towards the objective of obtaining the cross sections for the given reaction. However, at the outset, I would like to clarify that the term Data Analysis is not to be confused with the Analyser, which is a programming construct part of the analysis. I shall be elaborating on the entire framework specified earlier, with detailed plots and graphs illustrating the different processes that go into complete data analysis for a given run.

Another clarification must be made at this point. The chapter on analysis framework had been separated and put at the beginning of the report so that the framework was clear as the report progressed on the subjects of theory and calibration. It was important that the reader had the general outline of the experiment clear before reading the two chapters. Moreover, the reason this section was not included at the same time because it requires the input of the ground covered in theory as well as calibration. While it may seem slightly bewildering, the decision to split this explanation into two was taken with the objective of compiling a report which was easier to read through. With that matter cleared up, we begin by taking a look at the starting point of the analysis, i.e. the unpacked file.

Unpacked File

The unpacked file is a ROOT file (23) with the tree structure defined as follows –

```
SU_R      SD_R     DET1F     DET2F      PAD1E   PAD2E
SU_RI     SD_RI    DET1FI    DET2FI     PAD1T   PAD2T
SU_R_E    SD_R_E   DET1F_E   DET2F_E
SU_R_T    SD_R_T   DET1F_T   DET2F_T
SU_S      SD_S     DET1B     DET2B
SU_SI     SD_SI    DET1BI    DET2BI
SU_S_E    SD_S_E   DET1B_E   DET2B_E
SU_S_T    SD_S_T   DET1B_T   DET2B_T
```

The prefixes indicate the detector, where SU stands for the downstream S3 and so on for the other detectors (Naming conventions have been previously specified in Calibration). The suffixes are described below –

1. No Suffix (Example: SU_R or SU_S): This stands for the multiplicity. It indicates how many particles have hit this side of the detector. This is a number labelled **M**.
2. R & S: These stand for Rings and Spokes in the S3 detectors.
3. F & B: These stand for Front and Back strips in W1 detectors.
4. I: This stands for strip index and is an array with **M** entries. **M** runs from 1 to 16 for the W1s, 1 to 24 for S3 rings and 1 to 32 for S3 spokes.
5. E: This stands for Energy and is also an array. It stores the energy deposited in the given strip.
6. T: This stands for Time. It stores the time output from TDC and is also an array. This is the impact time when the particle hits the strip.

This unpacked file contains data in a well organised manner which can be used to closely monitor the input for the analysis framework. Any discrepancy which may appear anywhere in any stage down the line can be easily checked against the unpacked data to verify if it originates in the data acquisition or somewhere during the analysis. Even though the data is still in the form of counts vs. channel number, the importance of unpacked data cannot be understated.

Sorter

The purpose and concept of the sorter has been previously elaborated upon so we are not going to touch upon it again for brevity. What we would like to focus upon here is the execution of the step and how it transforms the data. As we know, the unpacked data is in the form of a ROOT tree entirely in terms of channel numbers and counts. The Sorter converts this unpacked root file into a sorted ROOT file.

The sorter uses the calibration files provided for each detector to do the calibration. It then performs the important function of matching to pinpoint the pixel that the particle hit. The concept of matching is illustrated with the help of the following figure –

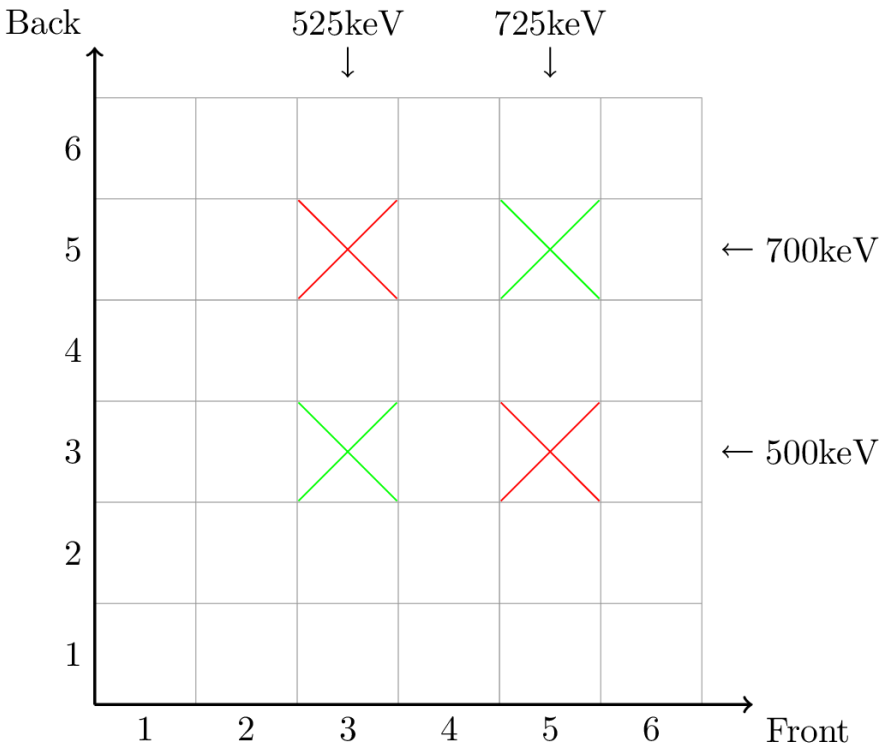

Figure 9 - Illustration of matching in a W1 detector

Assume a particle hits front strip 3 with an energy of 525 keV and another particle hits front strip 5 with an energy of 725 keV. The back strip 3 is hit by a particle of energy 500 keV and back strip 5 with energy of 700 keV. The two hits on front can correspond to any other strip on the back. So, the possible pixel positions of the two particles are (3,3), (5,3), (3,5) and (5,5). The Sorter selects the two combinations with the least energy difference, thus, selecting (3,3) and (5,5) in this case. This becomes the pixel associated with the particle and goes into the sorted file. This entire process is termed matching. Any specific details to be taken care of are taken care of during this step by specifying options in the “matcher.json” file. Consider an example of such a file –

```
{
  "DSD" : {
    "__GLOBAL__" : {
      "tolerance" : 100,
      "low_cut" : 100
    }
  },
  "SSD" : {
    "__GLOBAL__" : {
      "low_cut" : 100
    }
  }
}
```

This file specifies the global tolerance for all double sided detectors and the low cut for all double as well as single sided detectors. The tolerance is the maximum difference in energy between the front and back strips that can be accepted for a hit to be written in the sorted file. The low cut specifies the minimum energy the particle needs to have to be written in the sorted file. One can provide a variety of other options in the matcher file, including but not limited to specifying disabled strips, providing a high energy cut, specifying parameters specific for given strips, etc…

The process of calibration is fairly simple. The calibration file for each detector contains the slope and intercept for each individual strip calculated during energy calibration. This is simply applied to the data and the energy of the particles is obtained.

Sorted File

The sorted file is also a ROOT file. The tree is named a101 and has the following important branches –

```
mul
FI  BI
FE  BE
FT  FE
theta
phi
id
```

These are explained below –

1. mul – Multiplicity of the event, i.e. the number of hits in the given event. It is an array with **M** entries.
2. FI & BI – Front and back index, i.e. the strip index of the detector which was hit.
3. FE & BE – Front and back energy, i.e. the energy of the particle
4. FT & BT – Front and back time, i.e. the time at which the particle hit the strip
5. theta and phi – The spherical coordinates θ and ϕ.
6. id – Specifies which the detector was hit. 0, 1, 2 and 3 represent SD, SU, Det1 and Det2.

This is the first step where the program has done calculations for the user. The geometry of the setup has been utilised to calculate the spherical coordinates of the particle hits. At this point, we can see the standard histograms from the experiment such as the kinematic curve, detector hit patterns, etc... Once the sorting is done, the data is ready for the critical and lengthy process of particle identification.

The kinematic curve output seen at the end of sorting is shown in Figure 10 –

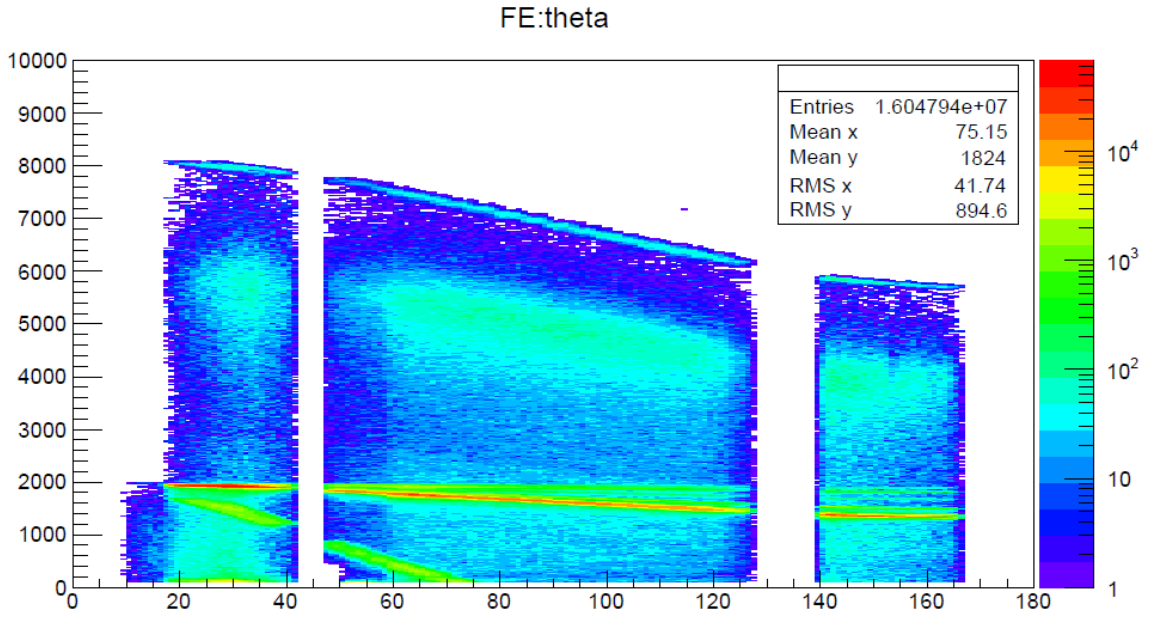

Graph 5 - Kinematic Curve Output after Sorting at 2 MeV Energy

One can clearly identify the salient features of the curve. At the top is the track of highest energy alpha particles from the ground state of ^{8}Be. The broad band starting around 6 MeV energy corresponds to the highest energy alpha particle in the excited state of ^{8}Be. At 2 MeV, one can see the track due to proton scattering of ^{11}B. Though it is not clear here, it diverges into several tracks as it reaches SU and can be used to identify impurities in the sample using the ROOT macro which can predict kinematic curves for scattering.

Identifier

As a tool, the Identifier was envisaged as a vital time saving component in the entire framework. Before it was part of the AUSAlib framework, the energy loss corrections, analysis, energy and tdc cuts were all part of one big analyser program. However, as previously mentioned, this would be time consuming when the analysis is being perfected. Thus the analysis was split into the Identifier

and the Analyser. In fact, the Identifier and the EventAnalyser were both finished in the first week of October and this study was almost like a beta test for the Identifier (alpha testing having been done by Michael and Oliver, the authors).

Conceptually, the Identifier was a leap from the previous version of code being utilised. That was because of its ability to assign all possible particle IDs, carry out the energy loss corrections and letting the Analyser deal with it. At the outset, it looks like the method is quite complicated. However, this complexity pays off big time at the time of analysis in terms of speed as well as ease of use.

So exactly how does the Identifier work? As mentioned in the schematic, the Identifier takes the sorted file as an input. So, it already has the detected energies and the positional information. Using the same, the first thing the identifier does is to carry out energy loss corrections. This is carried out using SRIM energy loss tables. The pixel position can be obtained given the geometry and the strip indices. This can be used to calculate the angle at which the particle enters the detector which can be used to calculate the effective dead layer. This dead layer is then used to calculate how much energy is to be added to the particle.

Once the energy loss correction has been done, the Identifier carries out the identification. It employs two methods to identify the particle. These are described briefly as follows –

1. dE cut: This cut determines how much energy has been deposited by the particle in the given detector. Then it considers each ion that the user has specifically asked to look for in a given reaction. If the ion cannot possibly deposit the amount of energy in the given detector (E.g. protons depositing greater than 3 MeV in a Silicon detector of 60 µm, as seen previously) then these particles are eliminated.
2. dE-E cut: This is a well-known cut on differential energy loss. In this kind of cut, a pad detector is placed behind the DSSD. This cut has not been implemented here so we don't discuss it in too much detail.

Once these cuts have been done, if the particle is not cut, the output is written along with the selected particle ID to the output file. After this, the next possible (user specified) particle undergoes the same process of energy loss corrections (assuming the particle identity) and identification cuts.

In several cases, a definitive identification cannot be made based on the above two cuts. In such a case, both the cases are written to the output. The advantage of doing this is that while identification cuts may not be able to differentiate between the given set of particles, further analysis written specifically for the experiment may be able to, based on other formulation. However, the analysis would then have the corrected energy of the particle available to work with saving valuable time.

The output of the identified file is quite similar to that of the sorted file, other than some renaming. However, a few key branches appear in this case. These are –

i. idmul – ID Multiplicity. This indicates the possible number of particles the hit could be. E.g. if a particle could be both a proton and an alpha, idmul is 2.
ii. A & Z – The mass and charge of the identified particle. These can be used to easily filter out a class of particles during analysis.

iii. energy – This is the energy of the particle. This is critical because the distinction between front strip and back strip energy is gone now. This is the energy of the particle after matching and energy loss corrections have been done.
iv. dlLoss & targetLoss – The energy corrections done for the dead layer and target respectively. Note that these have been done presuming the particle ID identified.

The output of the Identifier for the 2 MeV run can be seen in Figure 11 in the form of the kinematic curve from the run –

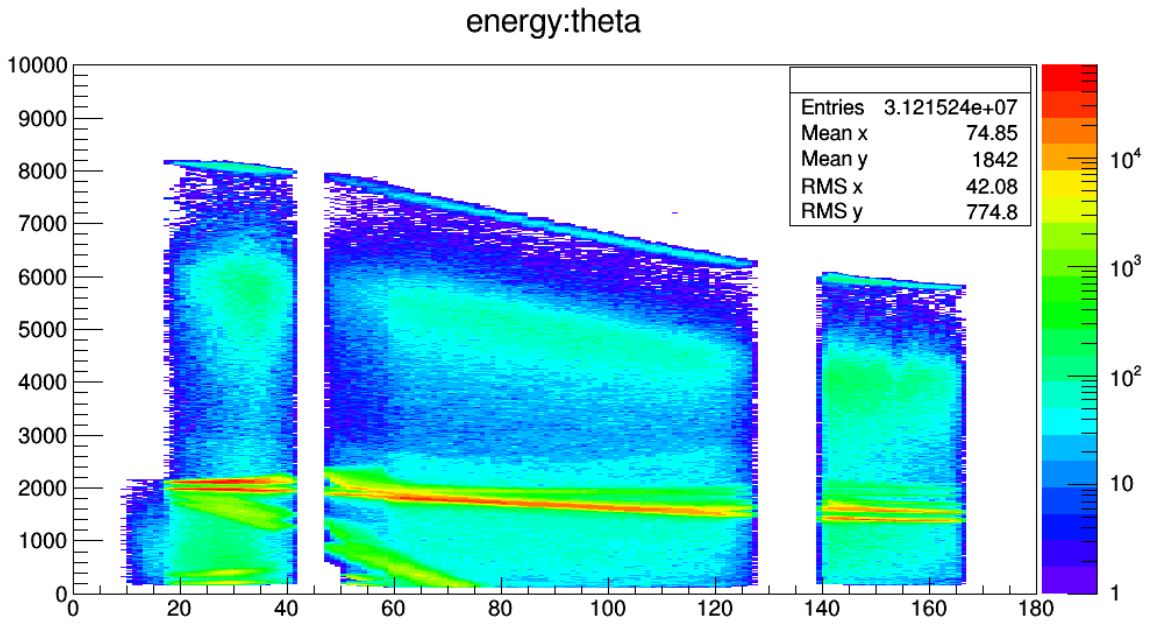

Graph 6 - Identifier output at 2 MeV Energy

Immediately, one can see that the total number of entries in this case is almost twice as many for the sorted file. This is because the Identifier has not been able to distinguish the large majority of particles and hence given an output with both the particles. This can be seen clearly in the proton track where the energy loss corrections, as explained previously, have split the expected proton scattering track into two, the other contribution coming from particles labelled as alpha by the identifier. These can now be rejected in the analysis.

Analyser

Once the identification is complete, the sorted and identified files are both used as inputs for the analyser. The analyser is the most experiment specific part of the analysis framework and is often built by a person with a particular experiment in mind. While the analyser can be generally modified to extend to other experiments, it is not exactly in spirit of the analysis framework which has been developed in the group.

I have written the analyser for this particular experiment with a lot of help and input from Michael and Oliver. The analyser output file is no longer a structured ROOT tree, but a collection of specific histograms which I would like to look into for pursuing specific objectives. The objective in my case was to examine the different runs, analyse them and calculate the differential cross section for the $^{11}B(p,\alpha)2\alpha$ reaction, differentiating between the ground state and the excited state of the ^{8}Be

intermediate nucleus formed. The two different methods employed for the same have been previously described in the framework. In this section, we would focus on the different histograms obtained from the analysis. Other than the above, the analyser also carries out EP and TDC cuts, which filter out a significant number of events.

The concept of the EP cut is that the total energy and momenta of the final particles must be equal to the energy and momentum of the initial beam particle. Clearly, this cut is only applicable in the cases where all the three particles have been detected, or as they are referred to, multiplicity 3 events.

The TDC cut on the other hand is a general constraint. It is the time window within which all detected particles must reach the detector, given that they originated from a triple alpha decay. This can be used to gate multiplicity two or three events. Higher multiplicity events are automatically rejected. The TDC cut has a width of ± 30 ns. It is applied to particles with a minimum energy of 500 keV.

Firstly, the method that was employed was to select only multiplicity 3 events, i.e. events where 3 particles have been detected. Through different cuts, it was confirmed that the observation of these particles is consistent with three alpha particles originating from an excited ^{12}C nucleus. Once these particles were selected, their energy and momentum were taken up. These were then transformed into the centre of mass frame and then summed over. The energy and momentum of the system must be conserved. This gives us the plot for EPCut, where the change in momentum is plotted against the change in energy of the system. Notice that change in energy denotes mass-energy since we are changing from the total energy of the beam (protons) to the final particles (alphas). A typical plot for an EPCut is shown below –

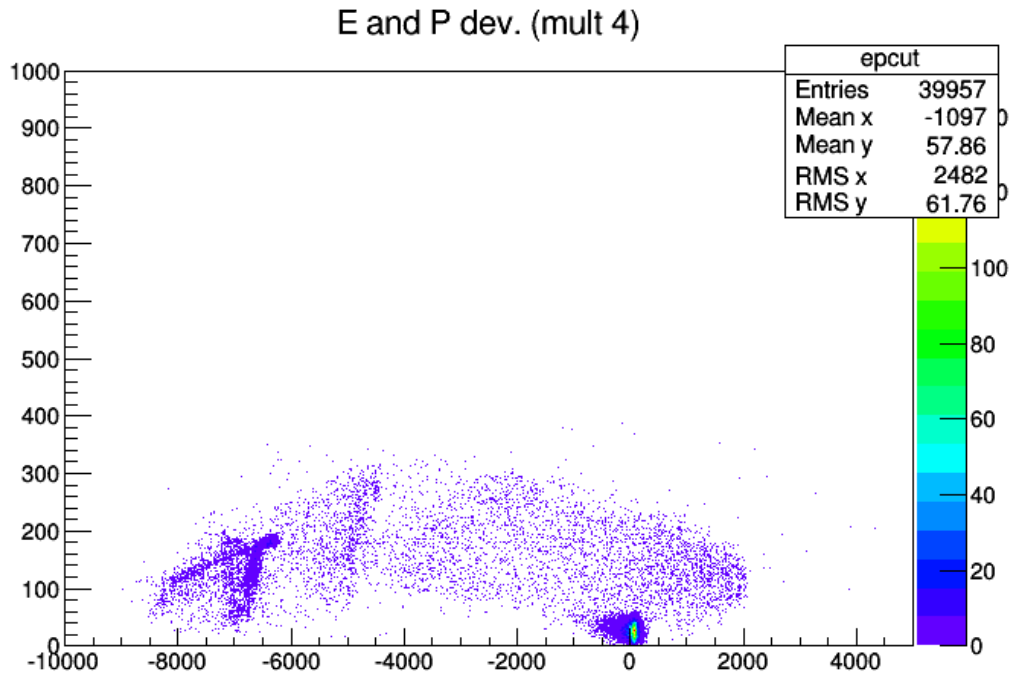

Graph 7 - EPCut at 2 MeV Beam Energy. The plot is essentially change in momentum (keV/c) vs. change in energy (keV)

We can clearly see the set of events which correspond to 3 alphas with energy and momentum conserved around the point (0,0). We can put a gate around the energy and momentum we wish to accept and consider only these events for further analysis. This is called an EPCut.

The EPCut plot is important from another perspective. Notice that for the system we have, while momentum has to be conserved, energy does not! For instance, if some of the energy is carried away by a gamma ray, then we would see another spot close to the X-Axis but with a significant loss of energy. This is how we look for gamma transitions using the detector setup. The drawback of this method is that we need to be able to detect all three particles after the decay and hence this becomes susceptible to detection efficiency. So, to detect gamma transitions using this method, we need a lot of statistics. In the run above, data has been taken only for 1 hour approximately. To obtain a statistically significant result, we need to take runs of the order of days at a single resonant energy. Such runs have been taken in fact and are being analysed by other people in the group.

The Analyser gives the following important histograms at the end of the analysis –

1. Kinematic curve – As always, the kinematic curve is an important tool as it can be used to gauge the calibrations of the setup at any point in the analysis. However, in this case, the kinematic curve is transformed into the centre of mass frame of reference so that the calculated energy cut-off can be used to isolate the highest energy alpha particles in the ground state decay. Kinematic Curves were computed after separation of ground state using the two methods mentioned in the analysis framework. Here we compare their results.
   First, we take a look at the kinematic curve obtained from the designated cut-off method. This is when we simply count all alphas above a cut-off energy as alphas from the reaction to the ground state of ^{8}Be. This curve is shown below zoomed in on the portion with the highest energy alphas from the ground state of ^{8}Be –

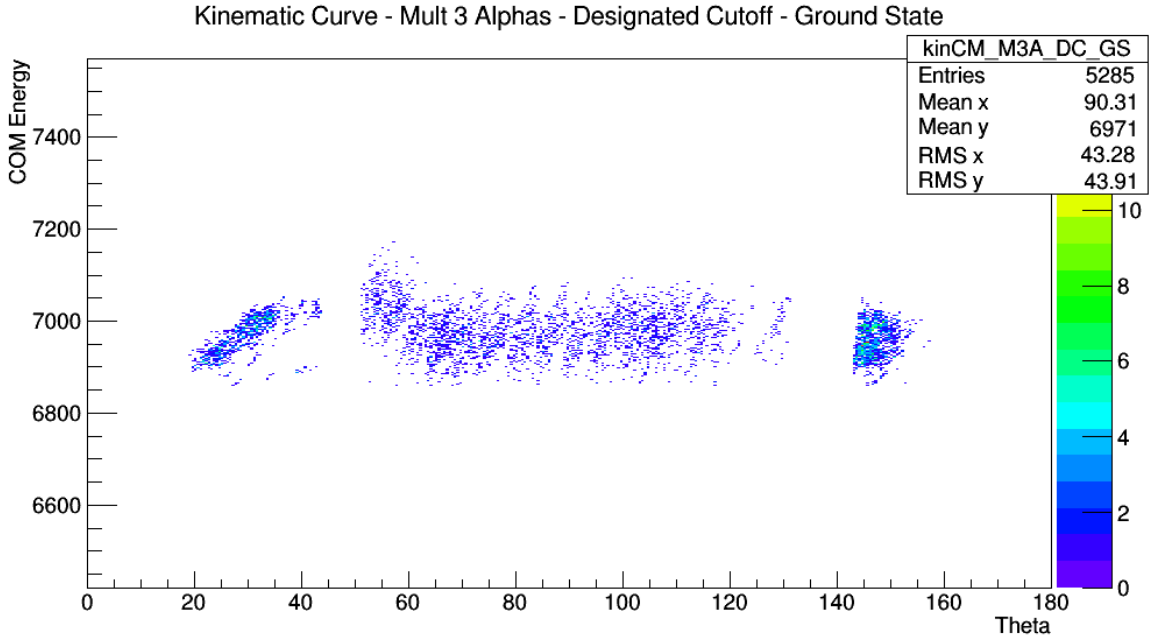

Graph 8 - Kinematic Curve in Centre of Mass frame at 2 MeV beam energy using the Designated Cut-off method

It is quite clear from the graph that the cut is quite clean. However, its accuracy is subject to the parameter chosen to account for any excess energy loss. The efficiency of the selection of this parameter needs to be verified through simulations.

Secondly, we look at the kinematic curve obtained using the invariant mass method. For this the square of the relative momentum between the two lowest energy alphas were gated over to select the three alphas. This method is much more selective and hence the possibility of false positives is much lower in this case. However, on the downside, we do not yet fully understand the efficiency of detection of all three alphas, as well as the efficiency of EPCuts. The kinematic curve for this method in the centre of mass frame is as follows –

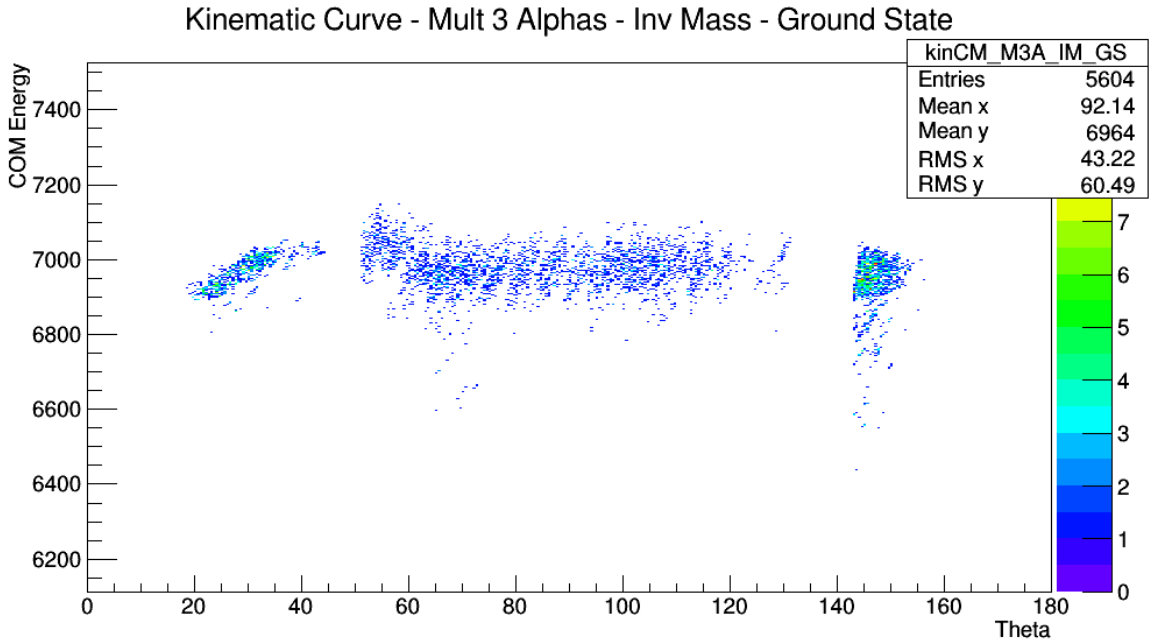

Graph 9 - Kinematic Curve in Centre of Mass frame at 2 MeV beam energy using the Invariant mass method

A comparison between the two curves reveals important details about the two methods used. The cut-off method provides a much cleaner curve when compared to the invariant mass method. It is not yet fully understood what is the origin of this long tail especially in SU in the curve obtained using the invariant mass method. Since the TDC and EPCuts have been applied, the system is highly constrained. It is possible that we need to constrain it further.

2. ThetaCM_DC_GS – This was a plot of total number of alpha particles vs. cos(θ), where each particle is the most energetic alpha in the decay through the ground state. These alpha particles are selected in the centre of mass frame using the method using an energy cut-off from calculations using separation energy and Q value of the alpha decay. This is shown in the graph below. This is essentially the differential cross section since it is counts vs. theta. However, we need to find the numerical proportionality for this graph. This is done with simulations later. In the graph below, we have selected an alpha particle if its energy is higher than the cutoff energy as calculated previously. This is irrespective of verification of the triple alpha reaction by detection of all three particles. The reason this method should work is because in this particular experiment, we do not expect particles from any other reaction channel at this energy.

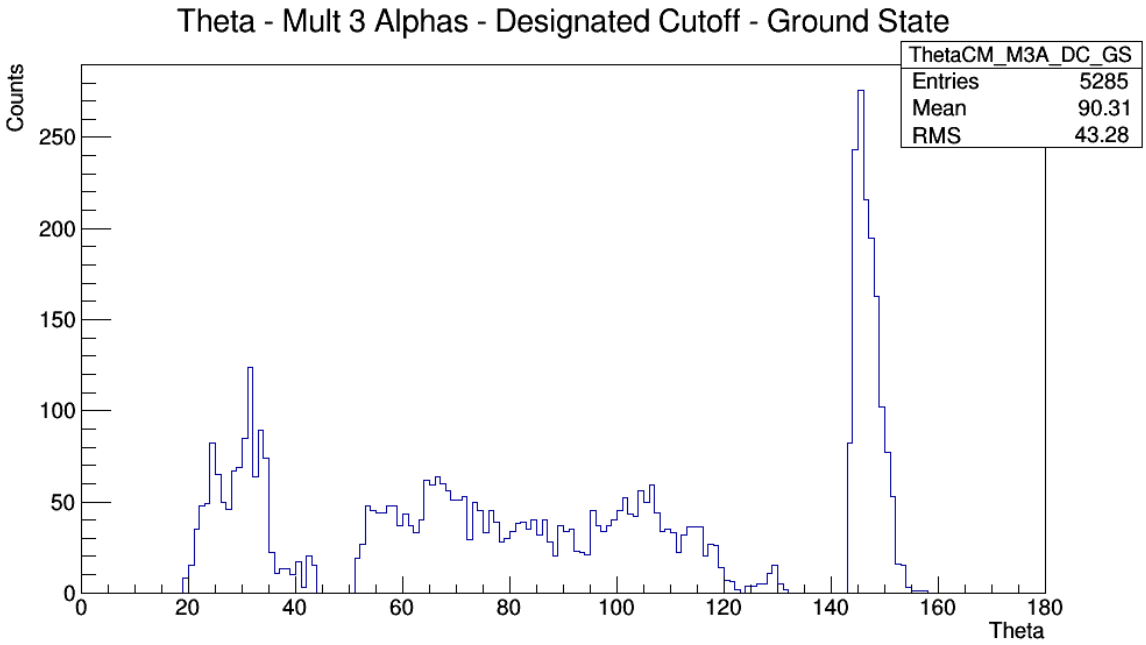

Graph 10 - Counts vs. Theta for highest energy alpha particles decaying through ground state of ^{8}Be at 2 MeV obtained using the Designated Cut-Off method.

The graph above shows that the distribution is a bit high in the upstream SU detector.

By comparison, the same graph using the invariant mass method is shown below –

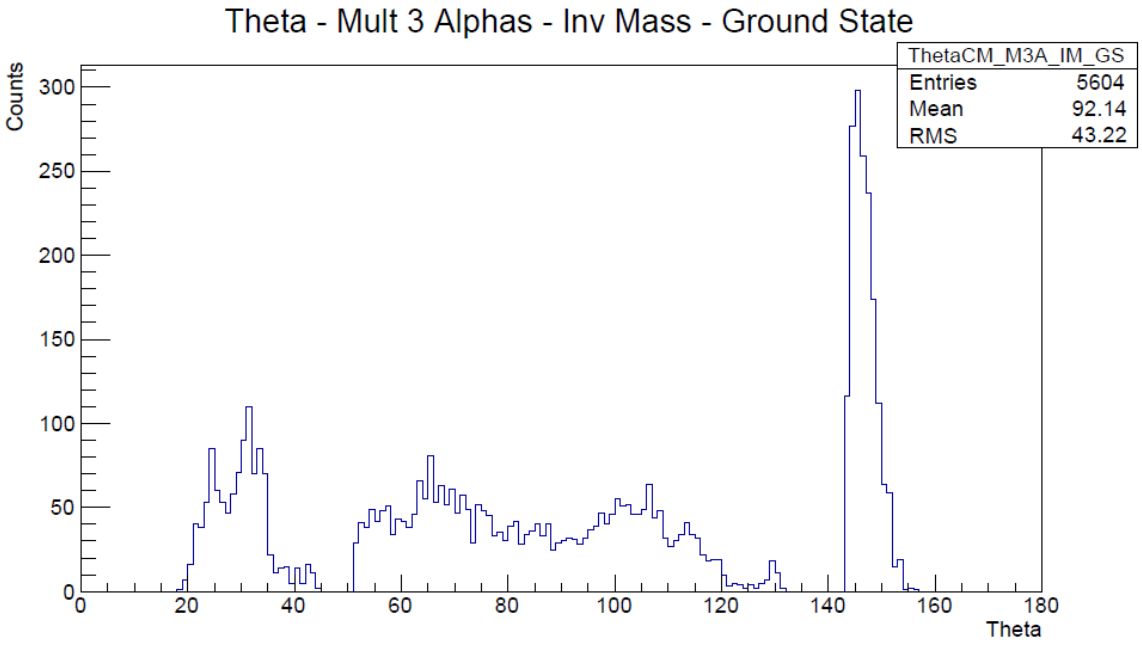

Graph 11 - Counts vs. Theta for highest energy alpha particles decaying through ground state of ^{8}Be at 2 MeV obtained using the invariant mass method.

Once again, we see the high count rate in SU.

At this point, one has to decide which method is better to calculate the cross section of the reaction. From what we know about the reaction, the ground state of the ^{8}Be nucleus is a not a broad state. Hence, we expect the track from the alpha particles emitted from ^{12}C going to ground state of ^{8}Be to

be fairly narrow. Also, given that the first excited state is 3 MeV above the ground state and has a width of 1.5 MeV, we expect the broad band of highest energy alpha particles from the first excited state to be isolated from the ground state. Other than these two reactions, there is only one channel left which may give alpha particles at this energy range, which is the rare (proposed) case where the ^{12}C decays directly into three alpha particles without going through an intermediate ^{8}Be nuclear state. In this case, the distribution of energy between the three alphas will be uniform. However, since this run has been taken for only one hour, this channel's contribution (if any) can be safely neglected. In the light of above facts, we can safely assume that further refinements are required to use the invariant mass method.

So, for now, we proceed by using the Designated Cut-off method and isolate the alpha particle track only for the ground state of ^{8}Be. In this case, we consider alphas from all detected multiplicity. Once an alpha particle has been identified as the highest energy alpha, we plot any other alphas detected along with it to obtain the kinematic curve. The final kinematic curve after isolating the track is shown below. The advantage here is that to get the cross section, we only need to count the highest energy alphas. This would give an accurate angular distribution since these are emitted directly by the excited ^{12}C. Moreover, a single alpha in this energy range corresponds to a single decay. So the efficiency of detection is purely geometric.

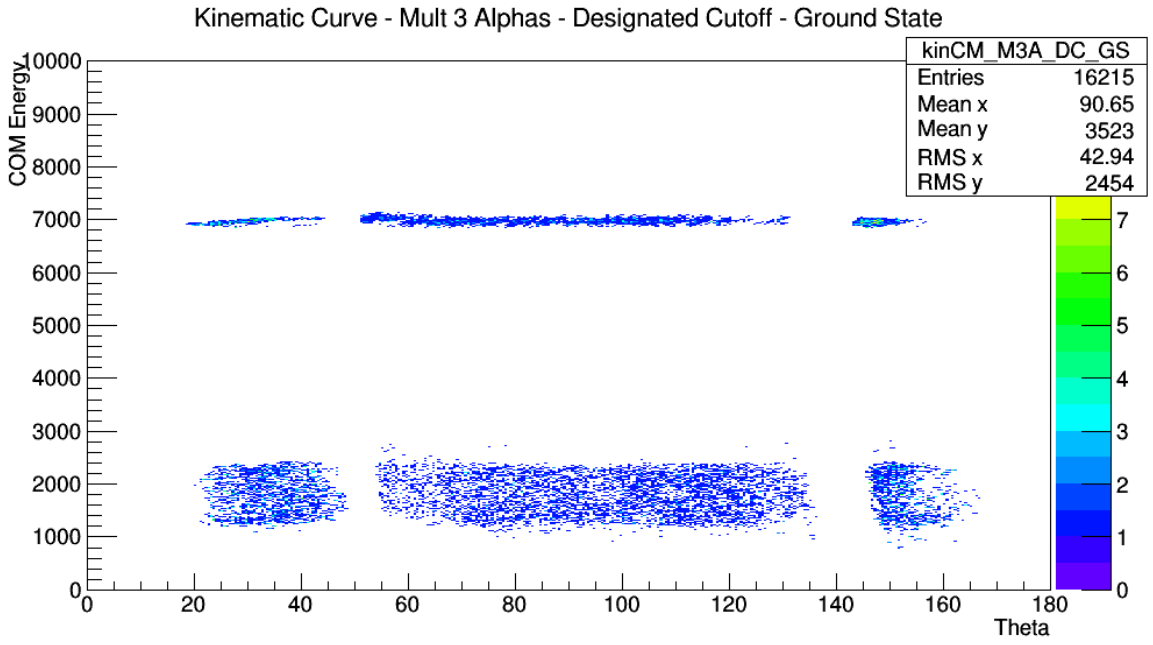

Graph 12 - Kinematic Curve at 2 MeV Energy for all alpha particles detected for the ground state channel of ^{8}Be. Note that for the purpose of cross section calculation, only the alphas in the track at the top are counted.

Having obtained the alpha particle spectrum, we now need to calculate the differential cross section. For this we bin the plot into a 1D histogram with the angle on X-Axis and correct for the solid angle of the pixel. To obtain the differential cross section from this, this histogram is simply divided by an identical histogram generated from a Monte-Carlo simulation and processed through the exact same analysis framework. Since the number of decays is known for the simulation, we can accordingly scale the differential cross section for real data.

Simulations

As previously mentioned, the cross section for the reaction under study was obtained by dividing the obtained spectrum (from the data) with a spectrum which was simulated with a known number of decays. However, the importance of simulations cannot be understated in the context of the analysis framework that has been developed at the nuclear physics group at Aarhus University. The simulations guide code development and provide a valuable tool to investigate any potential issues with real data.

The simulations use a pseudo-random number generator to generate a long sequence of random numbers distributed in the interval (0,1). As the name suggests, the sequence is not truly random but can be reproduced depending on the initial seed values provided to the generator. This may seem to defeat the purpose of a simulation, but on the contrary, it is beneficial to have a random number sequence which can be reproduced. For example, if simulating an event is causing a segmentation fault in the program, it would be difficult to debug if the error didn't show up the next time the reaction is simulated.

However, my concern in this experiment was not to worry about the inner workings of the simulation program, called SimX in AUSAlib, but to use it to systematically look at issues with my data. The output from SimX is essentially a ROOT file identical to the unpacked file obtained from real data. This file can then undergo the exact same treatment of Sorting, Identification and Analysis to give a final result which can be compared to real data. However, a crucial fact to note about SimX is that it can only simulate one reaction channel at a time. So, the output from SimX is far cleaner than that from actual data. This is beneficial since this helps us distinguish the data coming from different channels. We can easily merge two data files from different channels and analyse them together to see how the analysis works on the reaction as a whole, but the ability to individually examine each channel is priceless!

Now, since the analysis framework is clear, we quickly illustrate the output from a SimX file at different stages of analysis as an example, pointing out salient features along the way before proceeding to the final chapter describing results of the experiment.

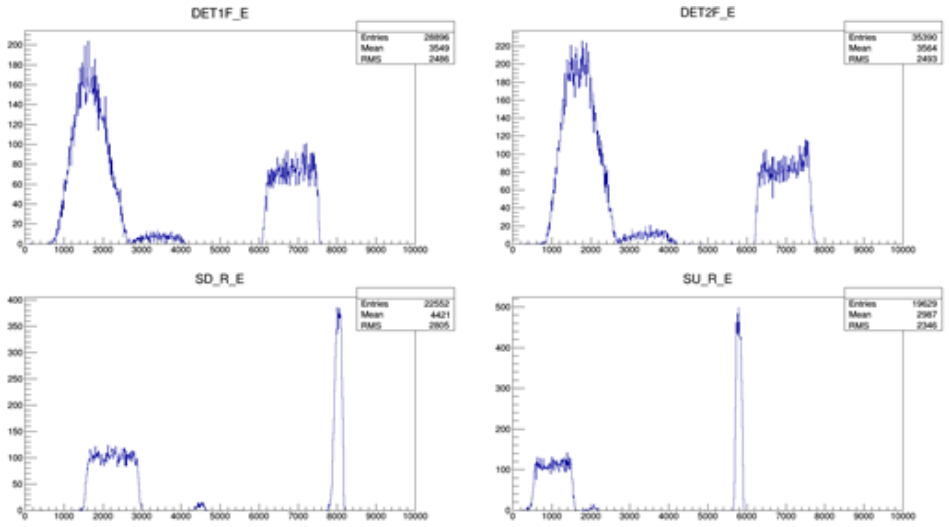

Graph 13 - Counts vs. Energy (keV) for unpacked data at 2 MeV from SimX. Clockwise from top left – 1. Det1 front strips 2. Det2 front strips 3. SU rings 4. SD rings

The output from SimX is shown in the figures above. If one looks back at the kinematic curves from the ^{8}Be ground state channel, these are easy to understand. The sharp peaks in SU and SD are due to small angular width of the variation. This combined with the fact that these are placed at extremely forward or backward angles means that the energy does not change too much in the angular range of the detector resulting in a sharp peak for the highest energy alphas. On the other hand, the fact that Det1 and Det2 are placed in an intermediate angular range and that they have a broad angular range result in significant broadening of the highest energy alpha peak.

When we sort this data, we get the following kinematic curve –

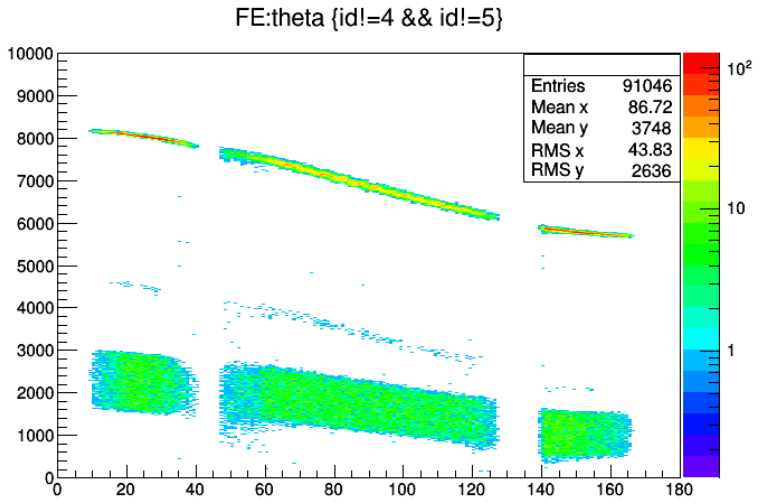

Graph 14 - FE vs. theta kinematic curve generated using SimX after Sorting at 2 MeV beam energy

One important feature to observe here is the number of events recorded. We have simulated a total of 100000 decays, but the graph above is showing close to 91000 entries. Since each decay gives three particles (any number of which may be detected) this amounts to roughly a third of decays being detected in whole or part. Nothing much else is of note here. All features have been described previously for the complete kinematic curve. Next, the identified kinematic curve is shown –

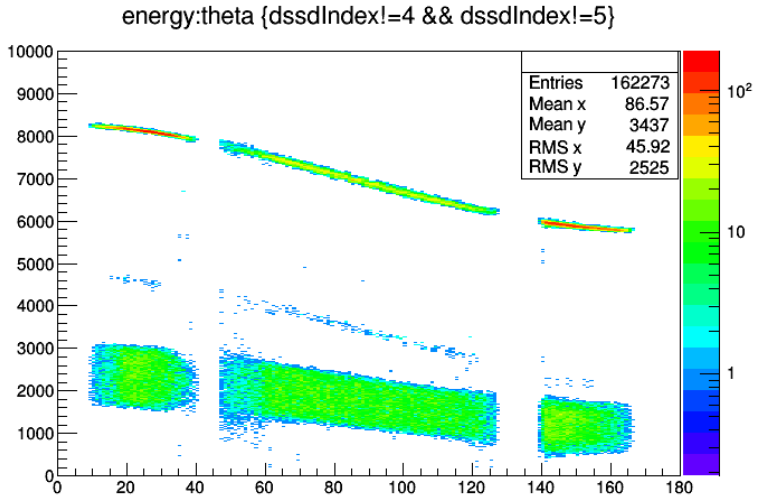

Graph 15 - energy vs. theta kinematic curve generated using SimX after identification at 2 MeV beam energy

At this point, we can look at another neat feature. We have seen previously that with the detector setup we have, the only unequivocal particle ID we can do is for particles in Det1 and Det2 above 3 MeV which, since they can't be protons, have to be alpha particles. The number of entries in this histogram is close to 162000, which when subtracted from twice of number of entries in the sorted histogram (≈ 180000) indicates the number of highest energy alphas detected in Det1 and Det2 in the ground state channel. While in this case, it may seem quite trivial, it is in fact a powerful proof of concept of the utility of the Identifier as an independent analysis stage. This is because while the current setup may have its limitations, the analysis framework can be easily extended to any future detector setup where such a technique could save a lot of time and effort. Let us not forget that the runs in this dataset are only one hour long and we need data for days to get statistically significant results!

Now that we have the output from the Identifier, we can go to the critical stage of analysis. At this point, we would like to use SimX to determine two things. Firstly, what should be an ideal cut-off parameter C to avoid selecting false positives? And secondly, what is the efficiency of the invariant mass method? First, we take a look at the kinematic curves obtained after the two different methods are applied. For convenience, they are both zoomed in on the relevant portion, i.e. the track of highest energy alpha particle. First, we look at the curve obtained from the designated cut-off method –

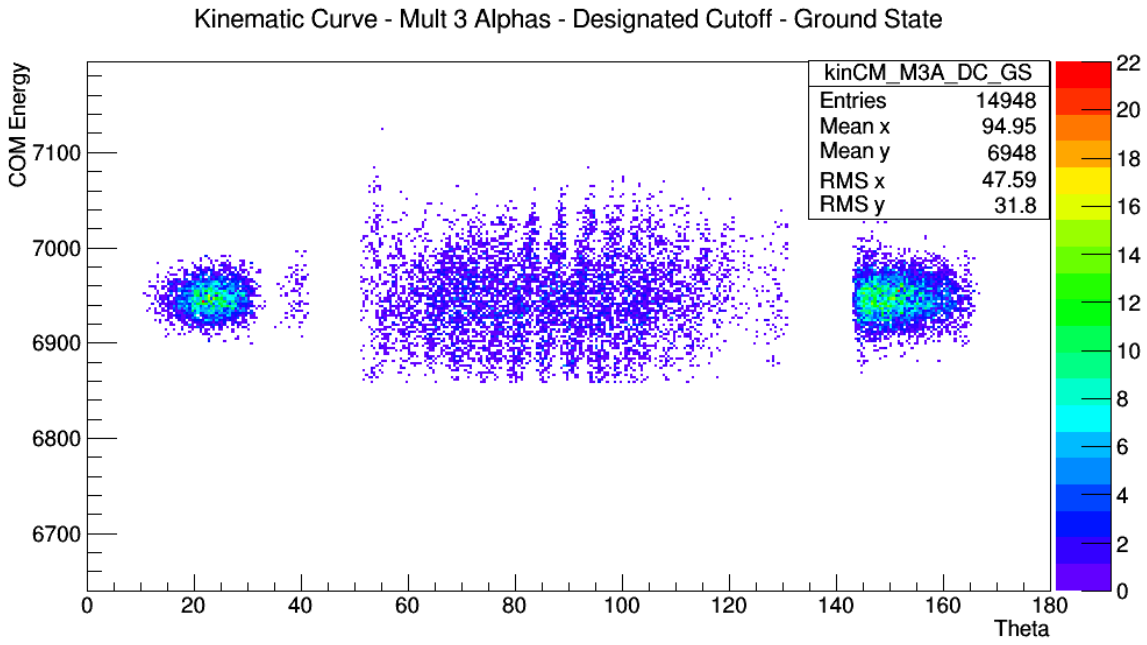

Graph 16 - COM Energy vs. theta Kinematic Curve from designated cutoff method after analysing data from SimX at 2 MeV beam energy.

Other than the fact that this has a lot more statistics than the curve from real data, it appears to be similar in terms of features of the histogram. This is more obvious from the 1D histogram with theta on the X-Axis as shown below –

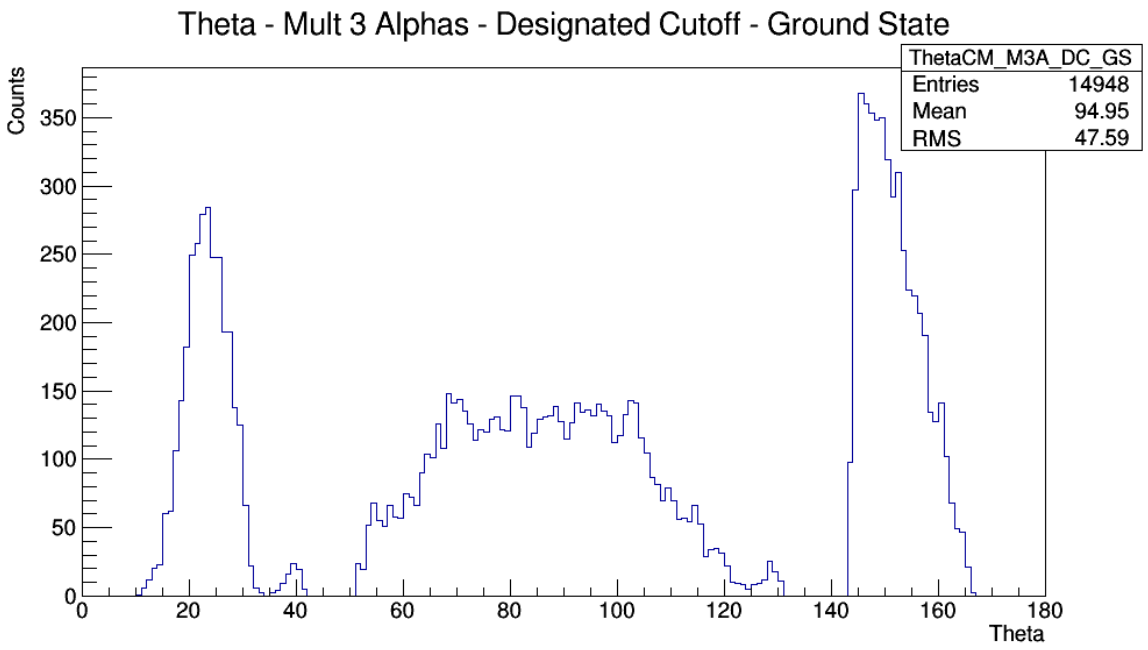

Graph 17 - Counts vs. Theta from the Designated Cut-Off method after analysis of SimX data at 2 MeV of incident beam energy.

In terms of broad features, this graph is quite similar to the one seen for real data. A larger count rate in the SD and SU as compared to Det1 and Det2 is seen here. However, when we compare the count rate in SU relative to other detectors, we see that it is similar to SD in this case, while previously it was significantly higher.

At this point it is important to point out a feature of SimX. The directionality of the reaction can be specified in SimX and is, by default, taken to be isotropic. So, the distribution seen here is as expected for an isotropic reaction. However, if the actual reaction is not isotropic, then we can expect certain differences in the two results. We can actually get around this problem of simulating the reaction distribution. The principle behind such a solution can be described as follows. First, the curve above is generated for both the real data as well as simulated data (with the simulation done isotropically). Then, these two curves can be divided to get a relative angular distribution of the real data. Then, a polynomial can be fitted to this relative angular distribution. This fitted polynomial can then be input to the simulation file to generate a dataset using this angular distribution. However, at the time of writing of this report, this has not yet been done.

Now, we can take a look at the same curve obtained using the invariant mass method. One should keep in mind that we can already expect certain entries to be cut out since the invariant mass method requires the detection of all three alphas. One cannot ascertain why the SU had a high count in real data since the other channels are not being simulated. Instead, we would like to see the fraction of decays in which all three particles have been detected. A single solution cannot be used to definitively say whether the efficiency of detection of all three particles is purely geometric in nature, but it certainly helps. Further analysis is required to definitively say if this efficiency is purely geometric in nature or there is some other physics behind it. With that in mind, we now look at the kinematic curve from the invariant mass method –

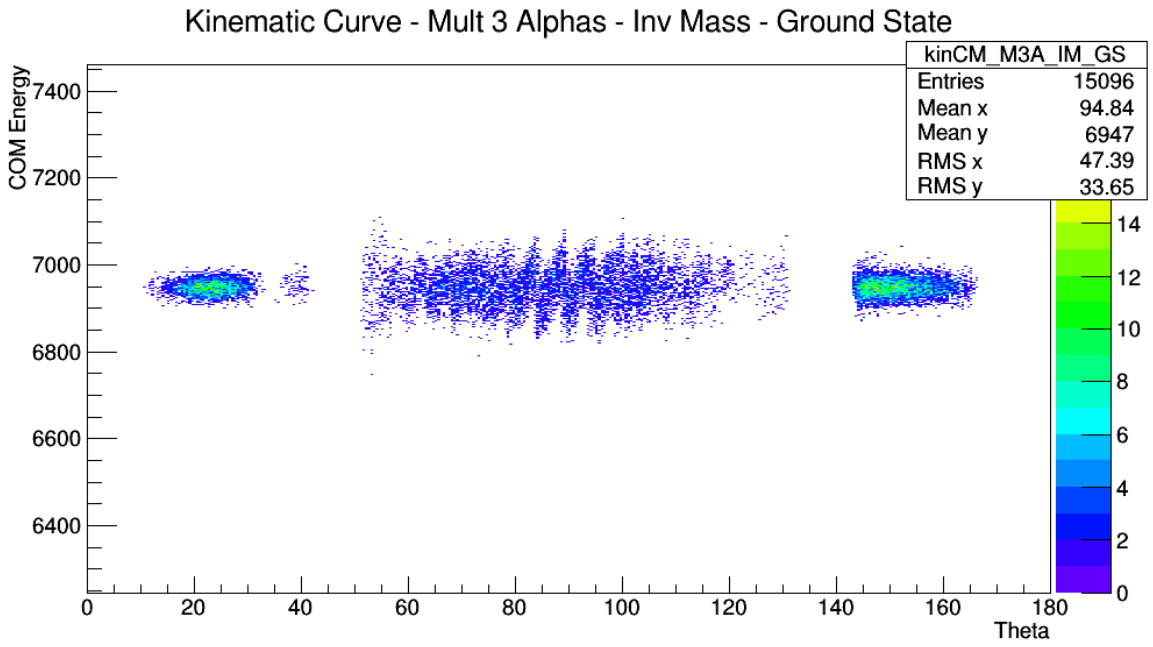

Graph 18 - COM Energy vs. theta Kinematic Curve from invariant mass method after analysing data from SimX at 2 MeV beam energy.

We can see that there are approximately 15000 entries which implies that roughly 15% of decays are being detected using this method. This is similar to what we see from the Designated Cut-off method. This becomes even more clear if we look at the Theta histogram as shown below –

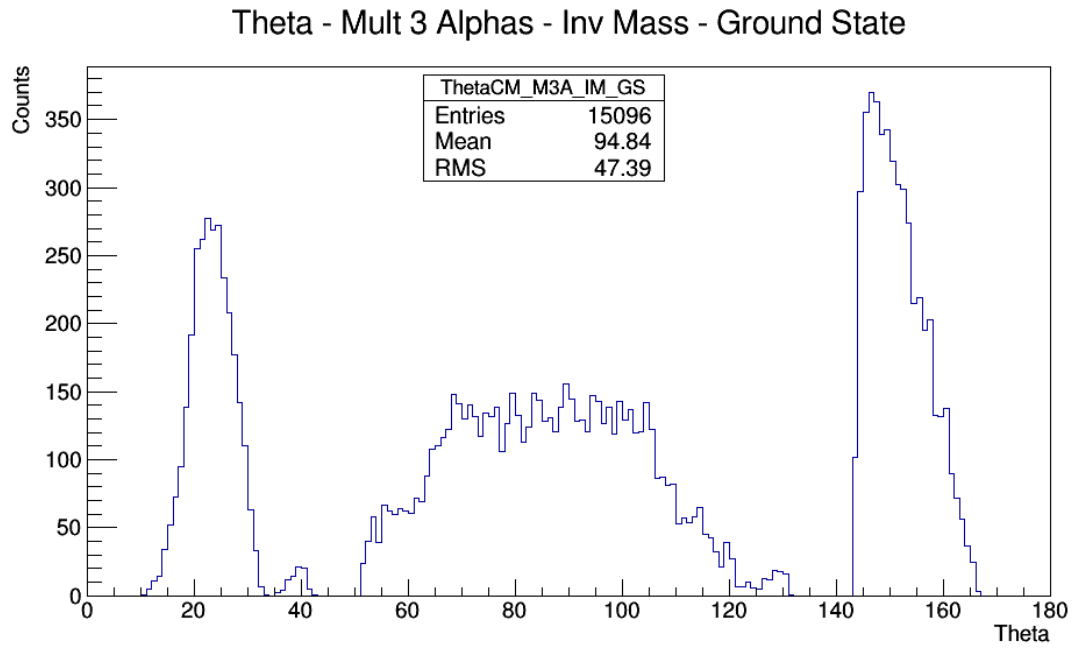

Graph 19 - COM Energy vs. theta Kinematic Curve from invariant mass method after analysing data from SimX at 2 MeV beam energy.

So, while the simulation looks similar in shape to real data, there are significant differences. The SU in the real data has a really sharp but tall peak as compared to the simulations. This appears to indicate an issue with the geometry of the setup.

Finally, to obtain the cross section, we divide the graph obtained from the Theta distribution in real data to that of simulations. This gives us the relative differential cross section between the two curves. But since the number of events in simulations is known, this can be scaled to the actual differential cross section. This plot is shown below –

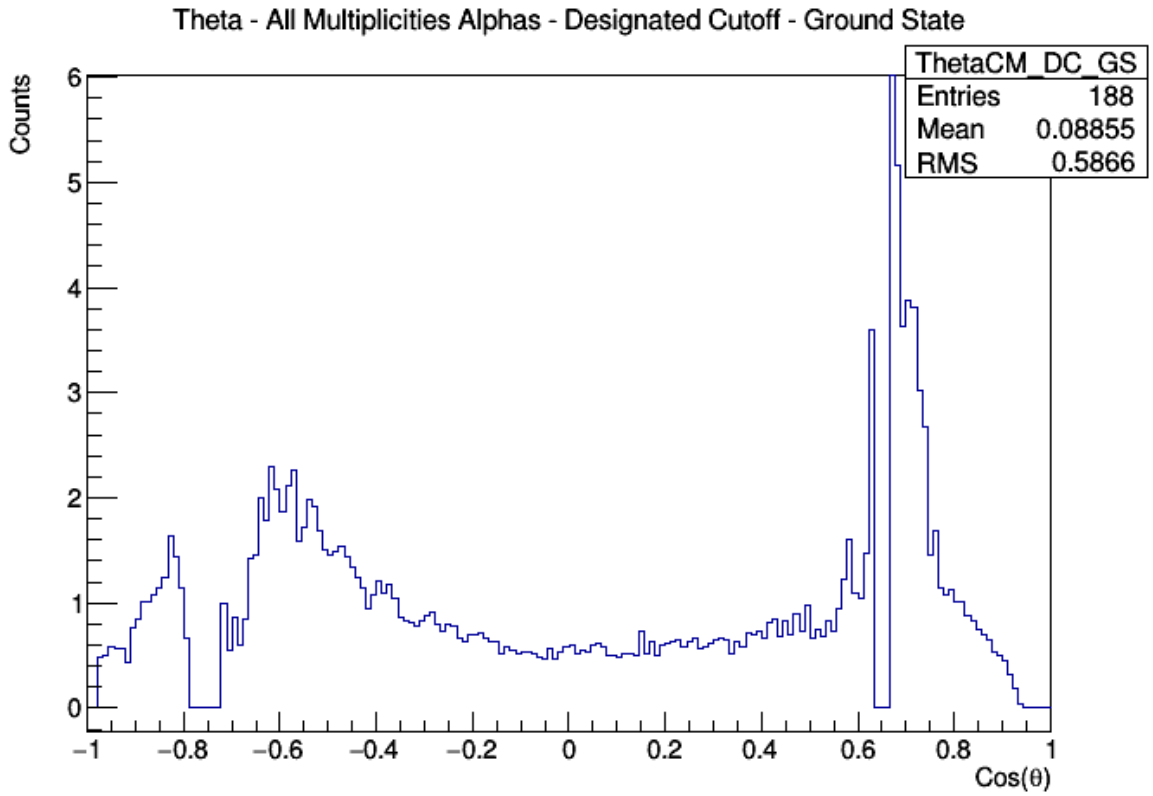

Graph 20 - Differential Cross Section - Counts vs. Theta for data at beam energy 2 MeV after Analysis

Here, the sharp peak is due to a bad data point around cosθ = 0.6

The distribution looks fairly smooth and can be used to fit a polynomial which can be used to improve the simulated directionality of the reaction.

This histogram is the final result of the Analysis. This has been calculated at every incident beam energy. This can be used to calculate the total cross section by correcting for solid angle and fitting with Legendre polynomials, but this exercise could not be due to shortage of time.

Conclusions and Outlook

In principle, obtaining the differential cross section is a successful end to the experiment and provides much needed closure after months of work. However, in practice, that is not really the case since several things can be done with the given data set. I am going to outline some of these things briefly.

Firstly, in the final analysed curves, the sharp peak in SU indicates that there is still an issue with the geometry of the setup. Towards the end of my stay, I had a brief communication with Michael who was also seeing similar issues with his own independent calculations. Given that the distribution is expected to be isotropic and is so near isotropic, it doesn't make sense that the reaction could be enhanced to this extent at one particular angle. On the positive side, having developed the framework thus far, selecting an isotropic channel now provides us with a new method to calibrate geometry. The geometry can be adjusted till the distribution matches an isotropic distribution. This can be implemented as part of AUSAlib framework in the future.

Another thing which I briefly touched upon was that the total reaction cross sections could be calculated from the differential cross sections obtained above. Once the geometry has been corrected, these curves can be fitted with Legendre Polynomials and normalised to give the total reaction cross section. This can be checked against previous work done by Segel, et al. and several other groups to confirm the accuracy of the analysis framework.

It is still required to establish the efficiency of different cuts taken here and consider what fraction of true events are cut out due to these. One also needs to consider the efficiency of detection of all three alpha particles and establish if it is purely geometric in nature or is there some deeper physics behind it. With the aid of higher statistics, possible gamma transitions could be spotted at known resonances. This can be seen easily with the help of the histogram used for EPCut as previously explained.

The data from the excited state of ^{8}Be state needs to be extracted as well. One helpful tool here could be the data around 670 keV. This is because as previously mentioned, this is a 2^{-} state and cannot decay to the ground state of ^{8}Be. Hence, this provides a great source of data where a channel is selected in real data and not just simulations. Any framework developed to extract ^{8}Be excited state data could be tested in this region with greater ease.

Ideally, I would like to continue to work remotely and at least establish the total cross sections of the transition through the ground state in ^{8}Be.

Finally, I would like to conclude this report by attaching the graphs of differential cross sections obtained for all the runs –

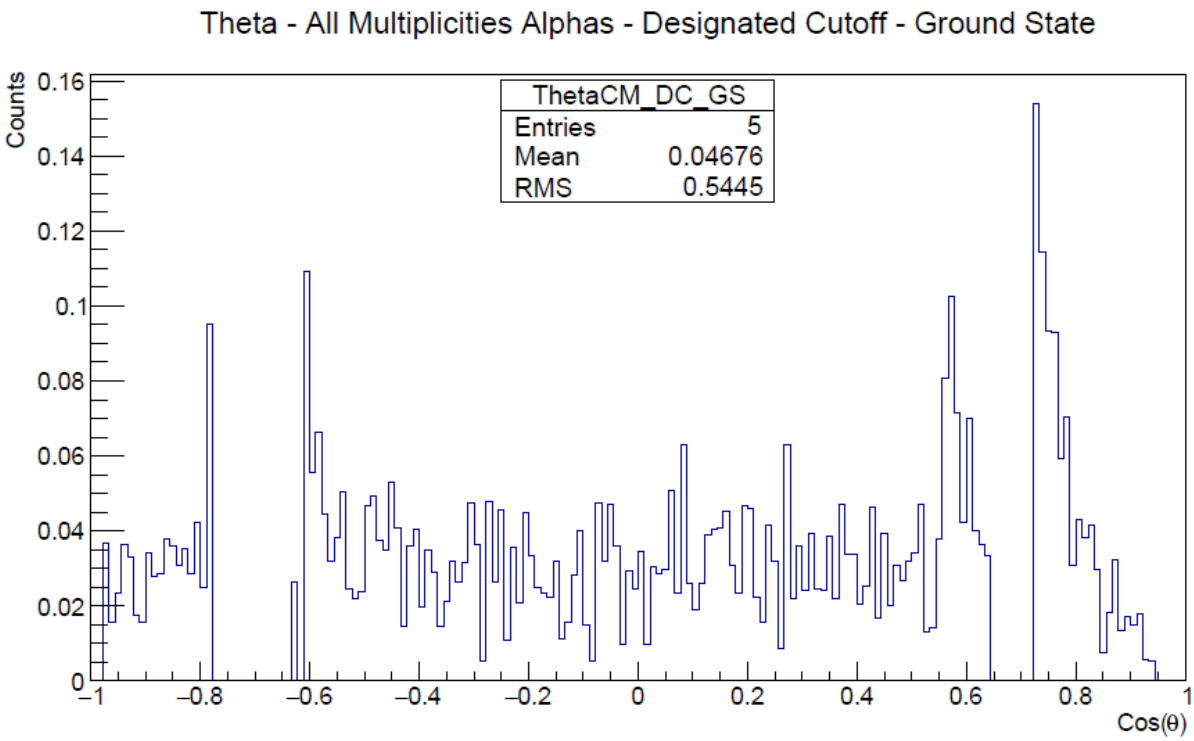

Graph 21 - Differential Cross Section at incident proton beam energy = 700 keV

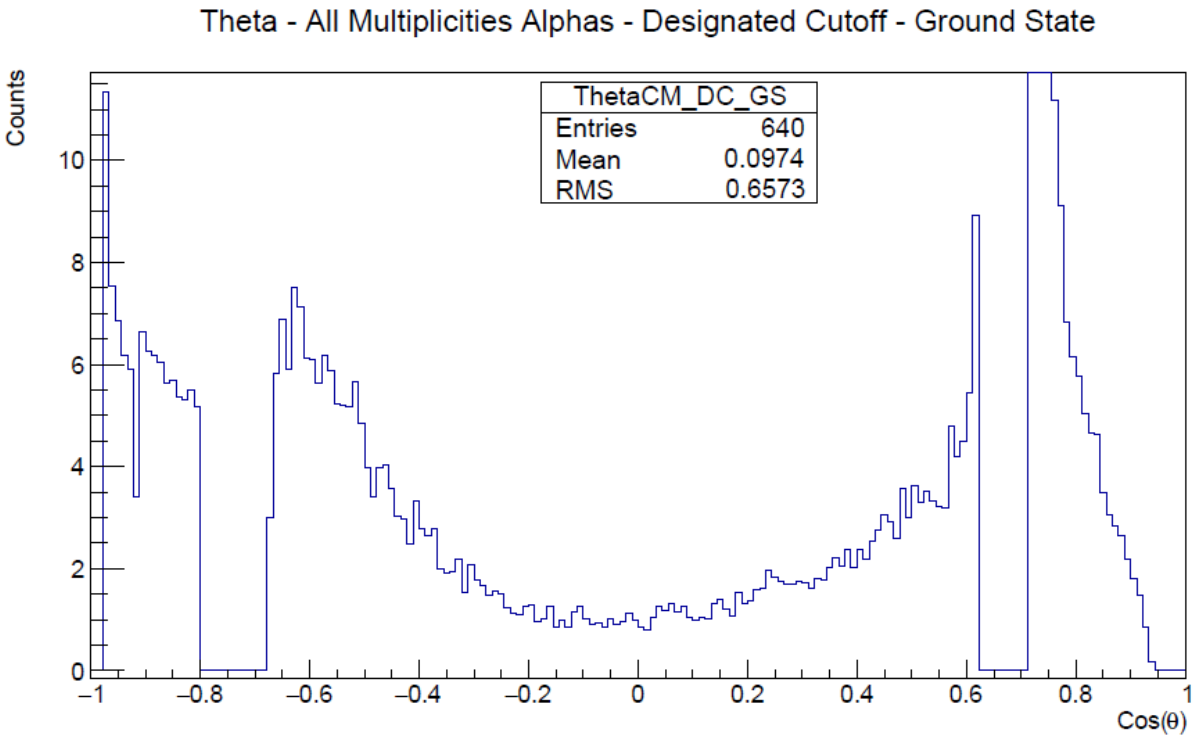

Graph 22 - Differential Cross Section at incident proton beam energy = 2650 keV

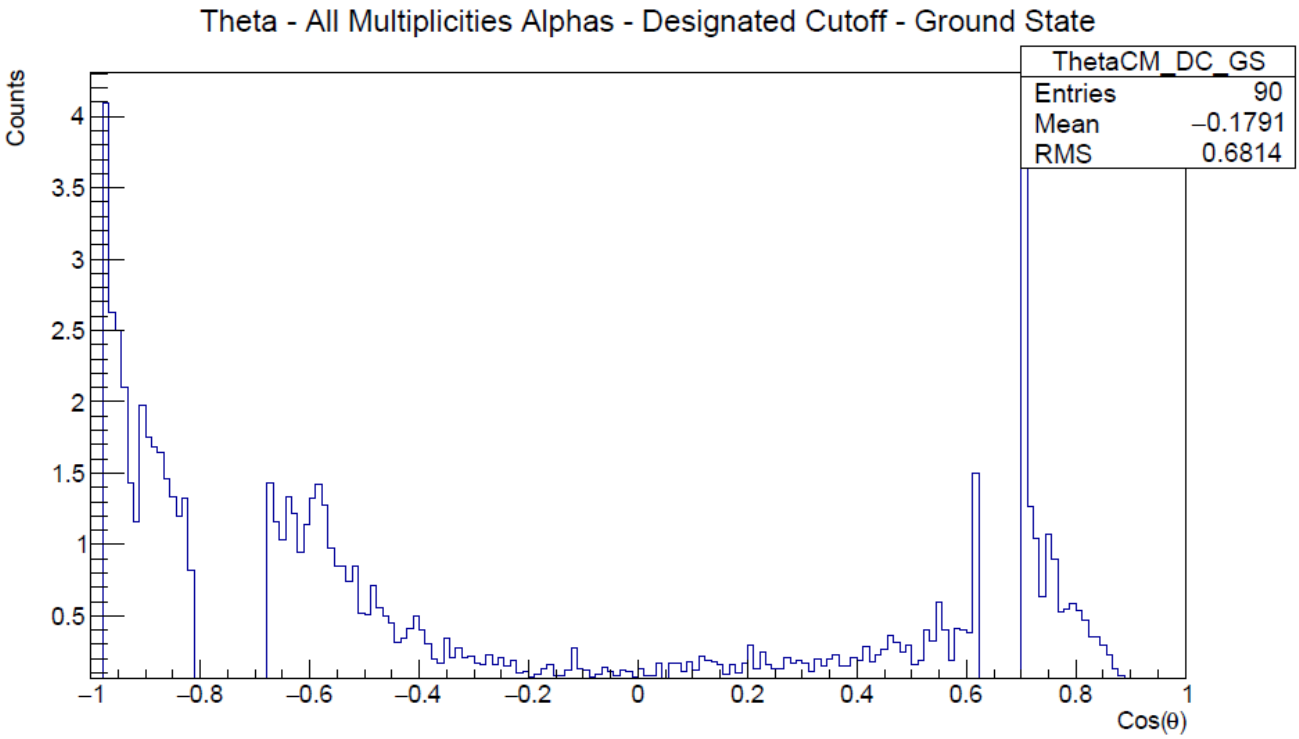

Graph 23 - Differential Cross Section at incident proton beam energy = 3500 keV

Bibliography

1. *On Nuclear Reactions Occurring in Very Hot Stars. I. the Synthesis of Elements from Carbon to Nickel.* **Hoyle, F.** s.l. : Astrphysical Journal Supplement Series, 1954, Vol. 1. ISSN 0067-0049.

2. *States in Carbon-12 Between 16.4 and 19.6 MeV.* **Segel, R. E., Hanna, S. S. and Allas, R. G.** 4B, s.l. : Physical Review, 1965, Vol. 139.

3. *Low energy cross sections for 11B(p,3α).* **Davidson, J. M., Berg, H. L., Lowry, M. M., Dwarakanath, M. R., Sierk, A. J., Batay-Csorba, P.** 1, s.l. : Nuclear Physics A, 1979, Vol. 315.

4. *Low-energy cross sections for 11B(p,3α).* **Becker, H. W., Rolfs, C. and Trautvetter, H. P.** 3, s.l. : Zeitschrift fur Physik A Atomic Nuclei, 1987, Vol. 327.

5. *New measurement of the 11B(p,α008Be bare-nucleus S(E) factor via the Trojan Horse method.* **Lamia, L. et al.** 1, s.l. : Journal of Physics G: Nuclear and Particle Physics, 2011, Vol. 39.

6. *Development of Boron-based materials for nuclear applications.* **Subramanian, C., Suri, A. K. and Murthy, T. S. R. Ch.** 313, s.l. : BARC Newsletter, 2010.

7. *Boron-Proton Nuclear-Fusion Enhancement Induced in Boron-Doped Silicon Targets by Low-Contrast Pulsed Laser.* **Picciotto, A. et al.** 3, s.l. : Physics Review X, 2014, Vol. 4.

8. *Suppresion of the chain nuclear fusion reaction based on the p + 11B reaction because of the deceleration of alpha particles.* **Shmatov, M. L.** 5, s.l. : Physics of Atomic Nuclei, 2016, Vol. 79.

9. *Boron detection using the nuclear reaction 11B(p,α)2α.* **Vollmer, M., Meyer, J. D., Michelmann, R. W. and Bethge, K.** 1, s.l. : Nuclear Instruments and MEthods in Physics Research Section B: Beam Interactions with Materials and Atoms, 1996, Vol. 117.

10. **Leo, W. R.** *Techniques for Nuclear and Particle Physics Experiments: A How-to Approach.* s.l. : Springer, 1994. ISBN: 3540572805.

11. MPR-16/L data sheet v. 7.0_01 mesytec. [Online] http://www.mesytec.com/products/datasheets/MPR-16.pdf.

12. MSCF-16 data sheet. v. 51 01. mesytec. [Online] http://mesytec.com/products/datasheets/MSCF16-F-V.pdf.

13. STM16+ data sheet. v. 2.4 01. mesytec. [Online] http://www.mesytec.com/products/datasheets/STM-16+.pdf.

14. V785 data sheet. Rev. 13. CAEN S.p.A. [Online] December 2012. http://www.caen.it/servlet/checkCaenManualFile?Id=8888.

15. V1190 data sheet. Rev. 13. CAEN S.p.A. [Online] July 2012. http://www.caen.it/servlet/checkCaenManualFile?Id=8657.

16. V830 data sheet. Rev. 4. CAEN S.p.A. [Online] January 2007. http://www.caen.it/servlet/checkCaenManualFile?Id=5281.

17. **Johansson, H. T.** The ucesb unpacker generator. [Online] 2010. [Cited: 11 May 2016.] http://fy.chalmers.se/~f96hajo/ucesb/ucesb_doc.pdf.

18. *The Ame2012 atomic mass evaluation.* **Wang, M. et al.** 12, s.l. : Chinese Physics C, 2012, Vol. 36.

19. **Bethe, H. and Ashkin, J.** *Experimental Nuclear Physics.* New York : John Wiley, 1953.

20. **Ziegler, J.** Stopping Range in Matter (SRIM). [Online] [Cited: 8 December 2016.] http://www.srim.org/.

21. *Compound Nucleus and nuclear resonances.* **Weisskopf, V. F.** s.l. : Helvetica Physica Acta, 1950.

22. **Krane, K. S.** Introductory Nuclear Physics. s.l. : John Wiley & Sons, 1987.

23. **Piparo, D., Quast, G. and Zeise, M.** A ROOT Guide for Students. [Online] July 2015. https://root.cern.ch/root/htmldoc/guides/primer/ROOTPrimerLetter.pdf.

24. [Online] [Cited: 11 December 2016.] https://wiki.kern.phys.au.dk/Targets.

25. [Online] Nuclear Physics Group, Aarhus University. [Cited: 12 12 2016.] https://git.kern.phys.au.dk/ausa/ausalib/wikis/Manual.

26. *Analytical function for fitting peaks in alpha particle spectra from Si detectors.* **Borels, G. and Collaers, P.** 10, s.l. : International Journal of Radiation Applications and Instrumentation., 1987, Vol. 38.

Table of Figures